UNIVERSIDAD NACIONAL DE COLOMBIA

A model independent study of sensitivity to CP violation in decays of charmed mesons to three-body final states

Sergio Javier Jaimes Elles

Universidad Nacional de Colombia
Facultad de Ciencias, Departamento de Física
Bogotá, Colombia
2021

A model independent study of sensitivity to CP violation in decays of charmed mesons to three-body final states

Sergio Javier Jaimes Elles

Trabajo de grado presentado como requisito parcial para optar al título de:
Magister en Ciencias, Física - Investigación

Director:
Ph.D. Diego Alejandro Milanés Carreño

Línea de Investigación:
Física de Partículas Experimental
Grupo de Investigación:
Grupo de Partículas FENYX-UN

Universidad Nacional de Colombia
Facultad de Ciencias, Departamento de Física
Bogotá, Colombia
2021

A mis padres,
Lenis y Javier.
Gracias por el apoyo constante y el amor incondicional.

Acknowledgements

Many thanks to all the friends, colleagues and family for the constant support and kind words of encouragement throughout this process. I'm extremely grateful to professor Diego Milanés for its continuous teachings and support, for the patience and the dedication invested. Many thanks to the cariocas, the LHCb Rio group and all its members. Special thanks to professor Alberto Correa dos Reis for its invaluable insight and guidance across this project. Thanks to every person that directly or inderectly contributed in some way to achieve this result.

Abstract

In the study of decays of mesons to three body final states the Dalitz plot analysis is a standard tool for the description of the phase space and CP violation searches in the quark sector. The technique applied for the study of these decays often depends on the model used for the description of the dynamics of the intermediate states. As an alternative, the Miranda procedure is used as a model independent method for detection of CP violation in decays of mesons. In this work we perform sensitivity studies using the Miranda procedure for the detection of CP violation on the decay $D^+ \to K^-K^+\pi^+$, using Monte Carlo generated samples.

Keywords: decay, CP vilation, Dalitz plot, charm quark, sensitivity, Standard Model, Miranda procedure.

Resumen

En el estudio de la desintegración de mesones en tres estados finales los diagramas Dalitz son una herramienta estandar para la descripción del espacio de fase y busquedas de violación CP en interacciones del sector de quarks. La tecnica usada para el estudio de estas desintegraciones amenudo depende del modelo usado para la descripción de la dinámica de los estados intermedios. Como una alternativa, el procedimiento de Miranda es usado como un método independiente del modelo para la detección de violación CP en desintegración de mesones. En este trabajo se realizó un estudio de sensibilidad a la detección de violación CP usando el procedimiento de Miranda en la desintegración $D^+ \to K^-K^+\pi^+$, usando muestras generadas por Monte Carlo.

Palabras clave: desintegración, violación CP, figura de Dalitz, quark encantado, sensibilidad, Modelo Estándar, procedimiento de Miranda.

Contents

1. Introduction

Violation of the Charge-Parity (CP) symmetry on weak interactions has been established and widely measured for different meson systems, in particular decays of K and B mesons. Due to the small amounts of CP violation (CPV) expected on the charm system within the Standard Model (SM), measurements of CPV related quantities require larger data samples and more refined statistical methods [1]. Just recently the first direct observation of CPV in decays of D mesons was observed by the LHCb collaboration, measuring the difference of the CP asymmetries for the decay channels $D^0 \to K^-K^+$ and $D^0 \to \pi^-\pi^+$ [2]. So far results coming from CPV in the quark sector seem to agree with SM expectations [3].

In the SM, CP violation appears from the complex phase in the mixing matrix of quarks in the charged weak interactions. Its measurement is of great interest as a constraint on the SM parameters but also since this symmetry relates matter and antimatter, it is known that a greater source of CPV is needed in the universe to account for the dominance of matter over antimatter. In this sense a deviation from expected SM values in the CP asymmetry may give us a hint on physics beyond the SM and new sources of CPV. As larger data samples of decays of heavy mesons to three final states and heavy baryons become available, studies on these modes turn of great interest, as their complicated structure may hide physics beyond the SM.

The study of decays of mesons to a system of three pseudo-scalars can be done using only two independent degrees of freedom and their phase space described by a 2-dimensional diagram, the Dalitz Plot (DP) [4]. The study of these decays is usually done on the isobar model description of the amplitudes, or its more formal description the K-matrix formalism [5]. Under these descriptions, fits to data on the decay amplitudes for the process and its CP conjugates are done and the CPV parameters measured. This approach although useful for measuring the CP observables of the SM, depends on the model used to describe the dynamics and is very demanding for analysis with great numbers of events. An alternative model independent approach using the direct comparison of the DP for a decay and its CP conjugate is proposed to measure the amounts of CP violation in a particular decay channel, the Miranda procedure [6, 7].

As expected SM effects of CPV on the charm sector are very small, large data sets are required to make such effects observable. As such, a sensitivity study is very important to determine the amount of CP violation that we would be able to observe in a data sample of given size. In this document an analysis of sensitivity to CPV on the decay $D^+ \to K^-K^+\pi^+$ for an estimated signal data size of the LHCb run II using the Miranda procedure is performed. The studies are done using a toy Monte Carlo generator that simulates the lineshape of the decay given a set of resonances parametrized by their magnitudes and relative phases. This complete set of parameters makes the amplitude of the decay, where CPV effects are introduced as relative differences in the magnitude or the phase between the decay mode and its CP-conjugate. By performing the Miranda procedure on set of 10 samples where every set has different levels of a asymmetry and different amounts of background contributions sensitivity to CPV is studied as the number of samples out of 10 in which a 5σ observation is possible. The study is also performed using three different binning schemes for the determination of the best binning strategy to be used on real data.

In the analysis performed on real LHCb Run II data sets, a data selection that ensures that no production asymmetries are introduced on the decay channel of interest is key to ensure that any asymmetries observed by the Miranda procedure come purely from CPV effects. For this, an analysis of the Miranda procedure is performed on the sidebands of the decays channel $D^+ \to K^-K^+\pi^+$ and the control channel $D_s^+ \to K^-K^+\pi^+$ is performed with the objective of studying any asymmetries coming from the background of the data set after data selection.

The present document is organized as follows. In chapter 2 a small review of the current theory behind CPV in the SM is presented, including a small discussion of the CP symmetry and its properties in physics. Chapter 3, discusses the Dalitz plot description of three-body decays and its main properties, a description of the Miranda procedure is presented. A short overview of the LHCb experiment can be found in chapter 4. The studies of sensitivity on toy Monte Carlo data for the decay $D^+ \to K^-K^+\pi^+$ are shown on chapter 5 with a study on the CPV of the sidebands obtained for real LHCb run II data is presented on chapter. Finally, conclusions of this study can be found in chapter 6.

2. CP violation in the Standard Model

The concept of Charge-Parity (CP) conjugation is key to the development of the Standard Model of particle physics. The violation of this symmetry by the weak interactions is an important characteristic of the model. By itself, P violation shows that only left-handed fermions can participate in weak interactions which defines the form of the operator used for the Lagrangian density description of the interaction, the $V-A$ lagrangian current. The violation of the combined symmetry CP by weak interactions appears from the mixing matrix in the interaction of quarks on the weak charged current. Measurements of CP violation serve as constraints of the parameters of the SM and a possible way into the discovery of new physics.

2.1. Symmetry

As understood by modern physics, symmetry is the invariance of a system under a given transformation. A system that after a particular physical transformation remains the same as before. This invariance allows to classify its behavior and understand some of its properties that at a first look might not be obvious. Because of its generality, this concept has become of central importance in the study of physical systems. From the rotation of an uniform sphere to gauge transformations in quantum field theory [8].

In classical physics, symmetry is associated with the invariance of the equations of motion under some transformation on the generalized coordinates. In quantum mechanics transformations are performed through the application of a unitary operator O on the state $|\psi\rangle$

$$|\psi\rangle \rightarrow |\psi'\rangle = O\,|\psi\rangle\,. \tag{2-1}$$

In that way, the normalization of the wave function is guaranteed and the probability is conserved

$$\langle\psi|\,O^{\dagger}O\,|\psi\rangle = \langle\psi|\psi\rangle = 1. \tag{2-2}$$

For a system that goes from an initial state $|i\rangle$ into a final state $|f\rangle$, such a transition is described by the matrix element $\langle f|\, S\, |i\rangle$. If a transformation O is performed, then the invariance of the system would imply

$$\langle f'|\, S\, |i'\rangle = \langle f|\, O^\dagger S O\, |i\rangle = \langle f|\, S\, |i\rangle\,, \tag{2-3}$$

which means that

$$O^\dagger S O = S \rightarrow [O, S] = 0. \tag{2-4}$$

This allows to relate the invariance of a system under a transformation O with its commutation to the S-matrix and by extension with the Hamiltonian ($[O, H] = 0$) [9].

Two types of physical transformations can be distinguished, Space-Time and Internal transformations. The first as the name suggests are transformations on the space-time coordinates of the state of the system, such as space translation, rotations or time reversal. Internal transformations act on the internal quantum numbers of the state like charge conjugation.

2.1.1. Parity

A particular space-time transformation important on quantum mechanics is parity. Parity transformation is the space reflection of all the coordinates as

$$\mathbf{x} \rightarrow \mathbf{x}' = -\mathbf{x}, \tag{2-5}$$

such that an unitary parity operator P acts on a wave function in the form

$$P\psi(\mathbf{x}) = \psi(-\mathbf{x}). \tag{2-6}$$

This operator has eigenvalues ± 1. In particular it is found that electromagnetic and strong interactions preserve parity but weak interactions do not ($[P, H_{weak}] \neq 0$).

The possibility of parity violation on weak interactions was first proposed by Lee and Yang in 1956 [10]. Their prediction was verified later on that same year by the measurement of angular distributions of electrons coming out of Co^{60} polarized nuclei in the famous Wu experiment [11]. By the early 1957 in a follow up experiment Garwin, Lederman and Weinrich confirmed the violation of parity in weak interactions by analyzing angular distributions from pion and muon decays [12, 13].

Total angular momentum is invariant under parity transformation, that is

$$[P, \mathbf{J}] = 0, \tag{2-7}$$

and orbital angular momentum is also invariant under parity ($\mathbf{L} = \mathbf{x} \times \mathbf{p}$). Since $\mathbf{J} = \mathbf{L} + \mathbf{S}$ for elementary particles, the parity of the spin operator is an intrinsic property that defines the parity of its wave function. This is called the intrinsic parity of a state.

2.1.2. Charge Conjugation

Charge conjugation symmetry appears naturally on quantum mechanics, with the introduction of special relativity and with it the existence of antiparticles. This symmetry is seen to be maximally violated by weak interactions [8]. The transformation associated with charge conjugation is the exchange of particles by its antiparticles, that is all internal charges (charge Q, isospin I, baryon number B, etc.) associated with the particular state change sign while the space-time coordinates remain unaffected.

Given an operator that transforms particle-antiparticle states

$$U_c \left|\pi^+\right\rangle = \left|\pi^-\right\rangle . \tag{2-8}$$

Being q_i any internal quantum number, electric charge Q, baryon number B, hypercharge Y, etc. Such an operator would transform as

$$U_c \left|q_i\right\rangle = \left|-q_i\right\rangle , \tag{2-9}$$

so that U_c and Q_i anti-commute

$$U_c Q_i \left|q_i\right\rangle + Q_i U_c \left|q_i\right\rangle = q_i \left|-q_i\right\rangle - q_i \left|-q_i\right\rangle \tag{2-10}$$

$$\{U_c, Q_i\} = 0. \tag{2-11}$$

Meaning that is not possible to find a simultaneous eigenstate of U_c and the internal quantum numbers Q_i. As a discrete transformation, the charge conjugation operator has eigenvalues ± 1 and as with parity transformation, electromagnetic and strong interactions have been observed to be invariant under charge conjugation but not weak interactions ($[U_c, H_{weak}] \neq 0$).

2.2. Standard Model

The Standard model of particle physics is build as a gauge invariant theory upon the Lie groups $SU(3)_C \times SU(2)_L \times U(1)_Y$ which breaks spontaneously into $SU(3)_C \times U(1)_Q$. This parametrization using gauge groups comes from considering the Lagrangian of the system invariant under a set of local gauge group transformations, that is transformations on the fields of the theory whose parameters are dependent of the space-time coordinates.

A first example of gauge groups is the Abelian group $U(1)$ on which Quantum Electrodynamics (QED) is constructed, the theory for the electromagnetic interaction. Extensions of

this are the non-Abelian groups like $SU(3)_C$ on which Quantum Chromodynamics (QCD) is constructed, this is the theory for the interaction of quarks mediated by eight vector bosons, the gluons, the theory for strong interactions. Weak interactions correspond to the gauge group $SU(2)_L$ and by the inclusion of a scalar multiplet and its potential, particles acquire mass while preserving gauge symmetry in the known Higgs mechanism.

2.2.1. Quantum Electrodynamics (QED)

Considering the Lagrangian density for a spin 1/2 free-particle (Dirac's Lagrangian)

$$\mathcal{L}_0 = \bar{\psi}(x)(i\gamma^\mu\partial_\mu - m)\psi(x). \tag{2-12}$$

In a similar way as in classical field theory, electromagnetic interactions can be introduced using the minimal coupling. In quantum field theory, this is given by the local transformations

$$\psi(x) \to e^{i\alpha(x)}\psi(x), \tag{2-13}$$

$$\bar{\psi}(x) \to e^{-i\alpha(x)}\bar{\psi}(x), \tag{2-14}$$

where to maintain the gauge invariance the derivative is replaced with a covariant derivative

$$\partial_\mu \to D_\mu = \partial_\mu - ieA_\mu(x). \tag{2-15}$$

Here the field $A_\mu(x)$ is introduced and transforms as

$$A_\mu(x) \to A_\mu(x) + \frac{1}{e}\partial_\mu\alpha(x). \tag{2-16}$$

In the description of electromagnetic interactions this will imply that the constant e corresponds to the absolute value of the electron charge and the field $A_\mu(x)$ is associated with the photon. Hence we introduce a photon kinetic term

$$\mathcal{L}_0^{EM} = -\frac{1}{4}F_{\mu\nu}(x)F^{\mu\nu}(x). \tag{2-17}$$

Such that $F_{\mu\nu} = \partial_\mu A_\nu - \partial_\nu A_\mu$ is the electromagnetic field tensor. Including this into our theory implies that the new Lagrangian density is given by

$$\mathcal{L}^{QED}(x) = \bar{\psi}(x)(i\gamma^\mu\partial_\mu - m)\psi(x) - \frac{1}{4}F_{\mu\nu}(x)F^{\mu\nu}(x) + e\bar{\psi}(x)\gamma^\mu\psi(x)A_\mu(x). \tag{2-18}$$

This is the Lagrangian of QED. Which represents a charged spinor field of mass m interacting with the electromagnetic field [14]. Which is shown through the interaction term

$$\mathcal{H}_{int}^{QED} = e\bar{\psi}(x)\gamma^\mu\psi(x)A_\mu(x) = j^\mu(x)A_\mu(x), \tag{2-19}$$

that will correspond to the conserved current according to Noether's theorem. The given transformation describes the unitary Abelian gauge group $U(1)$.

2.2.2. Yang-Mills theories and Quantum Chromodynamics (QCD)

Historically the observation of baryon states, hadrons composed of 3 constituent quarks, led to the introduction of three color charges to avoid violation of Pauli's principle. These color charges (red, green and blue) mean that each quark belongs into a representation of the gauge group $SU(3)_C$ [9]. In a similar way as in QED, the introduction of a local gauge symmetry with coupling constant e leads to the introduction of gauge vector bosons (the gluons). For strong interactions we start by generalizing this idea to the case where we have more than one type of state given by the color charge (q_a, $a = r, g, b$). With the local gauge transformation

$$q_a \rightarrow q_a^{'} = e^{\frac{i}{2}\lambda_A \Lambda_A(x)} q_a. \tag{2-20}$$

Here the transformations

$$U = e^{\frac{i}{2}\lambda_A \Lambda_A(x)}, \tag{2-21}$$

are unitary and have determinant 1. This makes the states q_a a representation of the color SU(3) group, and λ_A, $A = 1, ..., 8$ the eight Gell-Mann matrices [15]. Starting from the Lagrangian density for free quarks

$$\mathcal{L}_0 = \bar{q}^a (i\gamma^m u \partial_\mu - m) q_a. \tag{2-22}$$

For the three quark families (u, d, s). As before if we want our Lagrangian to be invariant under the given transformation, we need to replace the usual derivative by a covariant derivative given by

$$\partial_\mu \rightarrow D_\mu = \partial_\mu - \frac{i}{2} g_s \lambda_A G_{A\mu}. \tag{2-23}$$

here g_s corresponds to the coupling constant of the strong interaction and the vector fields $G_{A\mu}$ are the gluon fields, the generators of the interaction. The gluon strength tensor is

$$G^A_{\mu\nu} = \partial_\mu G_\nu - \partial_\nu G_\mu + i g_s f^{ABC} G^B_\mu G^C_\nu. \tag{2-24}$$

Here an extra term is included compared to the EM case for the strength tensor which will result in an interaction term between gluons, in strong interactions the vector bosons also carry color charge.

Non-Abelian gauge theories were first proposed by Yang and Mills in 1954 [16]. It corresponds to a generalization of the gauge symmetry used for constructing QED in which interactions are described using a special unitary group of degree N, SU(N). Hence the case

of strong interactions is described with the non-commutative $SU(3)_C$ gauge group where the Lie Algebra is given by

$$[t^A, t^B] = if_{ABC}t^C. \tag{2-25}$$

Being the eight t_a the 3×3 traceless matrices that generate the Lie group. These are related to the Gell-Mann matrices by

$$t_A = \frac{1}{2}\lambda_A. \tag{2-26}$$

Considering all of these properties the complete Lagrangian for QCD will be

$$\mathcal{L}^{QCD} = \bar{q}^a(x)(i\gamma^\mu(\partial_\mu + ig_s G^\alpha_\mu(x)\frac{1}{2}\lambda_\alpha) - m_a)q_a(x) - \frac{1}{4}G^\alpha_{\mu\nu}(x)G^{\mu\nu}_\alpha(x). \tag{2-27}$$

Here the kinetic term for the gluon field was also included.

2.2.3. Weak Interactions

First indications of the existence of a weak interaction came from the study of β-decays and the postulation of the neutrino by Pauli. The theoretical approach towards a theory for weak interactions starts with the proposition of Fermi's Lagrangian for the description of this particular type of decays [17, 18]. As other similar processes began to appear it became evident the need for a theory for this new type of interactions. The discovery of parity non-conservation proposed by Lee-Yang and later measured by Wu gave a more clear insight of the properties of this interaction [10, 11]. Later on, it was be proved that parity non-conservation also applied to the decay of pions and for the different decay modes of the K^+ which will be known as the $\tau - \theta$ problem [4]. All this experimental information gave hints for the existence of a new kind of interaction that not only violated parity but also has relatively long decay times and with a very small range. With all of this the introduction of a Vector minus Axial $(V - A)$ type of current made its way to describe an effective Lagrangian for weak interactions as the only possible coupling that can reproduce the desired helicity results observed from experiment. This is done using a current-current interaction term of the form

$$\mathcal{L}_{eff}(x) = -\frac{G_F}{\sqrt{2}}J^\dagger_\lambda(x)J^\lambda(x) + h.c. \tag{2-28}$$

Here G_F is the universal Fermi coupling constant and the $J^\lambda(x)$ current has the vector minus axial form given by

$$J^\lambda(x) = \bar{\nu}_l\gamma^\lambda(1 - \gamma_5)l + \bar{u}\gamma^\lambda(1 - \gamma_5)d'. \tag{2-29}$$

Each term corresponds to the leptonic and hadronic currents respectively. The interaction between up and down type of quarks is given by the mixing matrix which will be discussed in depth in the next section.

The inclusion of the factor $(1-\gamma_5)$ in the interaction shows that only negative chirality states are allowed on weak interactions, which goes in accordance to observations for the helicity of the electrons in β-decays [9]. This theory is able to make a very good description of some phenomena present in weak interactions at low energies but is not self-consistent, it violates unitarity at lowest order and is non renormalizable. Besides this, the presence of neutral weak currents were established from the measurements of neutrino-electron scattering at CERN [19]. Considering all these characteristics of the weak interactions the gauge theory proposed for their description is the composed symmetry $SU(2)_L \times U(1)_Y$ that is spontaneously broken into $U(1)_Q$ by the Higgs mechanism in which the gauge bosons acquire mass.

2.2.4. Electro-weak unification

In the SM at high energies there is a single $SU(2)_L \times U(1)_Y$ symmetry that is spontaneously broken by the vacuum expectation value of a doublet H into $U(1)_Q$ in what is known as the Higgs mechanism. Through this mechanism we are able to build a model for weak interactions that includes the $V-A$ form with intermediary massive vector bosons and a massless photon that mediates electromagnetic interactions while also accounting for charged and neutral weak interactions. It is through this mechanism that the gauge bosons and the fermions acquire a mass while preserving universality and renormalizability of the theory.

The $SU(2)_L \times U(1)_Y$ symmetry is used as a model for the unification of electromagnetic and weak interactions. This group is generated by 4 vector bosons, 3 generators from $SU(2)_L$ and one from the hypercharge $U(1)_Y$, they are $W^{\alpha}_{\mu\nu}$ and $B_{\mu\nu}$ respectively with coupling constants g and g'.

The fermionic sector of the theory is described by left-handed doublets for leptons and quarks

$$L^i_L = \left\{ \begin{pmatrix} \nu_{eL} \\ e_L \end{pmatrix}, \begin{pmatrix} \nu_{\mu L} \\ \mu_L \end{pmatrix}, \begin{pmatrix} \nu_{\tau L} \\ \tau_L \end{pmatrix} \right\} Q^i_L = \left\{ \begin{pmatrix} u_L \\ d_L \end{pmatrix}, \begin{pmatrix} c_L \\ s_L \end{pmatrix}, \begin{pmatrix} t_l \\ b_L \end{pmatrix} \right\}, \tag{2-30}$$

and the right handed $SU(2)$ singlets

$$L^i_R = \{e_R, \mu_R, \tau_R\} \tag{2-31}$$

$$u^i_R = \{u_R, c_R, t_R\} \tag{2-32}$$

$$d^i_R = \{d_R, s_R, b_R\}. \tag{2-33}$$

Introducing the Higgs multiplet

$$\phi(x) = \begin{pmatrix} \phi^{(+)}(x) \\ \phi^{(0)}(x) \end{pmatrix}, \tag{2-34}$$

the symmetry breaking will be generated by including the potential

$$V(\phi) = (D_\mu \phi)^\dagger \left(D_\mu \phi) - \lambda(|\phi|^2 - \frac{\nu^2}{2} \right)^2. \tag{2-35}$$

with the covariant derivative

$$D_\mu \phi = \left[\partial_\mu + \frac{i}{2} g W_\mu^a \tau^a H + \frac{i}{2} g' B_\mu \right] \phi, \tag{2-36}$$

that couples the scalar doublet to the SM gauge bosons. The Higgs potential induces a non-vanishing vacuum expectation value (vev) for ϕ, i.e. $|\langle 0|\, \phi\, |0\rangle| = \nu/\sqrt{2}$ that spontaneously breaks the symmetry. The vacuum of the theory breaks the symmetry but the Lagrangian is still invariant under it. Parametrization of the Higgs multiplet makes explicit the mass eigenstates for the gauge bosons $W_\mu^\pm$, Z_μ while allowing the inclusion of mass terms for the fermions without breaking gauge symmetry [20].

The Yukawa couplings of the Higgs doublet to the fermions are given by

$$\mathcal{L}_Y = -y_d \bar{Q}_L \phi d_R - y_u \bar{Q}_L \bar{\phi} u_R - y_l \bar{L}_L \phi l_r + h.c. \tag{2-37}$$

After electroweak symmetry breaking the fermion mass terms arise in the form $-m_e(\bar{e}_L e_L + \bar{e}_R e_R)$ with $m_e = y_e \nu/\sqrt{2}$, given by the Yukawa couplings y_f [21].

2.3. CKM matrix

The interactions in the electro-weak sector do not mix between quark families in the flavour basis but once we transform into the mass basis it can be noted that the $W_\mu^\pm$ couplings do have mixing terms given by the mixing matrix V

$$\mathcal{L}_{mix} = \frac{e}{\sqrt{2} sin\theta_w} \left[W_\mu^+ \bar{u}_L^i \gamma^u (V)^{ij} d_L^j + W_\mu^- \bar{d}_L^i \gamma^u (V^\dagger)^{ij} u_L^j \right], \tag{2-38}$$

here θ_w is the Weinberg angle and $sin^2\theta_w \approx 0.231$, is the angle by which SSB rotates the B_μ, W_μ^3 gauge bosons into the physical Z_μ^0 and A_μ mass eigenstates.

This mixing matrix is known as the Cabibbo-Kobayashi-Maskawa (CKM) matrix

$$V = \begin{pmatrix} V_{ud} & V_{us} & V_{ub} \\ V_{cd} & V_{cs} & V_{cb} \\ V_{td} & V_{ts} & V_{tb} \end{pmatrix}. \tag{2-39}$$

It is a complex unitary matrix with 9 degrees of freedom that can be represented using three rotation angles and six phases. Using re-definitions of the quark fields five of the six phases can be removed. Leaving us with only four independent degrees of freedom. With this description taking as δ the remaining phase and θ_{12}, θ_{13} and θ_{23} as the rotation angles in the ij-flavor plane, the CKM matrix can be parametrized as

$$V_{CKM} = \begin{pmatrix} c_{12}c_{13} & s_{12}c_{13} & s_{13}e^{-i\delta} \\ -s_{12}c_{23} - c_{12}s_{23}s_{13}e^{i\delta} & c_{12}c_{23} - s_{12}s_{23}s_{13}e^{i\delta} & s_{23}c_{13} \\ s_{12}s_{23} - c_{12}c_{23}s_{13}e^{i\delta} & -c_{12}s_{23} - s_{12}c_{23}s_{13}e^{i\delta} & c_{23}c_{13} \end{pmatrix}. \tag{2-40}$$

The rotation angles in the mixing matrix are considerably small, meaning that the CKM matrix is close to a diagonal. In the Wolfenstein parametrization we redefine the matrix in terms of the four real parameter A, λ, ρ, η by taking

$$s_{12} = \lambda, \quad s_{23} = A\lambda^2, \quad s_{13}e^{i\delta} = A\lambda^3(\rho - i\eta). \tag{2-41}$$

With this we can rewrite the CKM matrix as an expansion in terms of λ. At the order λ^6 the CKM matrix in the Wolfenstein parametrization is [22]

$$V_{CKM} \approx \begin{pmatrix} 1 - \frac{\lambda^2}{2} - \frac{\lambda^4}{8} & \lambda & A\lambda^3(\rho - i\eta) \\ -\frac{\lambda^6}{16}\left[1 + 8A^2(\rho^2 + \eta^2)\right] & & \\ -\lambda + \frac{\lambda^5}{2}A^2\left(1 - 2\rho - 2i\eta\right) & 1 - \frac{\lambda^2}{2} - \frac{\lambda^4}{8}\left(1 + 4A^2\right) & A\lambda^2 \\ & -\frac{\lambda^6}{16}\left(1 - 4A^2(1 - 4\rho - 4i\eta)\right) & \\ A\lambda^3\left(1 - \rho - i\eta\right) & -A\lambda^2 + A\lambda^4(1 - 2\rho - 2i\eta) & 1 - \frac{\lambda^4}{2}A^2 \\ +\frac{\lambda^5}{2}A(\rho + i\eta) & +\frac{\lambda^6}{8}A & -\frac{\lambda^6}{2}A(\rho^2 + \eta^2) \end{pmatrix}. \tag{2-42}$$

From this parametrization it is observed how the imaginary terms in the charm sector appear at the order of λ^5 while in the bottom appear at the order of λ^3. Hence it is expected that CP violation will be very small in decays of charmed hadrons within the SM.

The condition of unitarity in the CKM matrix implies a relation like

$$V_{ud}V_{ub}^* + V_{cd}V_{cb}^* + V_{td}V_{tb}^* = 0. \tag{2-43}$$

If we define the parameters $\bar{\rho}$ and $\bar{\eta}$ as

$$\bar{\rho} + i\bar{\eta} = -\frac{V_{ud}V_{ub}^*}{V_{cd}V_{cb}^*}, \tag{2-44}$$

the unitarity of the CKM matrix can be represented graphically in the complex plane as shown in figure **2-1**. Where the internal angles are given by

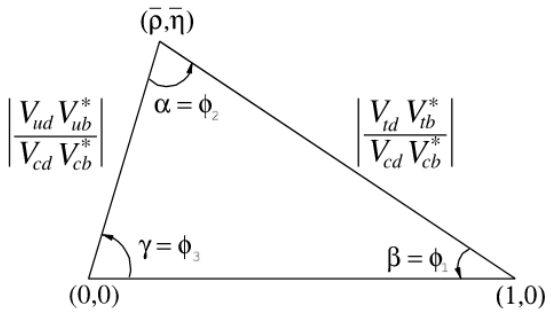

Figure **2-1**.: Unitarity triangle on the $\bar{\rho} - \bar{\eta}$ plane.

$$\alpha = arg\left(-\frac{V_{td}V_{tb}^*}{V_{ud}V_{ub}^*}\right), \tag{2-45}$$

$$\beta = arg\left(-\frac{V_{cd}V_{cb}^*}{V_{td}V_{tb}^*}\right), \tag{2-46}$$

$$\gamma = arg\left(-\frac{V_{ud}V_{ub}^*}{V_{cd}V_{cb}^*}\right). \tag{2-47}$$

Fits on these values from measured CKM parameters help to constraint the SM mixing parameters in the quark sector in search for new physics. The CKMfitter group [23] fit is shown in figure **2-2**.

Most recent average values give

$$\lambda = 0.22453 \pm 0.00044, \quad A = 0.836 \pm 0.015 \tag{2-48}$$

$$\bar{\rho} = 0.122^{+0.018}_{-0.017}, \quad \bar{\eta} = 0.355^{+0.012}_{-0.014}. \tag{2-49}$$

and magnitude values of the CKM matrix are

$$|V_{CKM}| = \begin{pmatrix} 0.97401 \pm 0.00011 & 0.22650 \pm 0.00048 & 0.00361^{+0.00011}_{-0.00009} \\ 0.22636 \pm 0.00048 & 0.97320 \pm 0.00011 & 0.04053^{+0.00083}_{-0.00061} \\ 0.00854^{+0.00023}_{-0.00016} & 0.03978^{0.00082}_{-0.00060} & 0.999172^{+0.000024}_{-0.000035} \end{pmatrix}. \tag{2-50}$$

taken from the Particle Data Group Review [3]. The inner angles of the unitarity triangle are

$$\alpha = 91.7^{+1.7\circ}_{-1.1}, \quad \beta = 22.56^{+0.47\circ}_{-0.40}, \quad \gamma = 65.80^{+0.94\circ}_{-1.29}, \tag{2-51}$$

taken form the CKMfitter results [23].

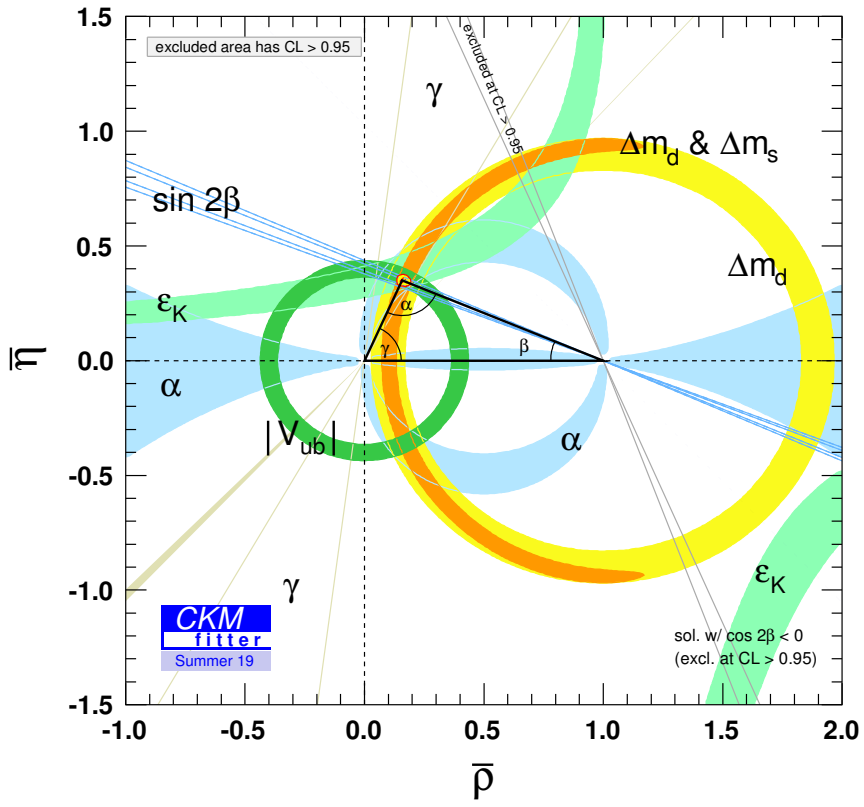

Figure **2-2**.: Unitary triangle on the $\bar{\rho}-\bar{\eta}$ plane with the fitted results obtained by the CKM fitter group [23].

2.4. CP violation

Parity non-conservation under weak interactions suggests that to have a complete left-right symmetry of the interactions the complete mirror reflection will be the CP transformation. This seems to recover the apparent asymmetry of the weak interaction currents, since it seems to act in the same way in left-handed particles as in right-handed anti-particles, the corresponding CP conjugate. CP transformation in addition to the time inversion completely inverts all the space-time coordinates of our Lagrangian. CPT theorem tell us that any Lorentz invariant local Lagrangian must respect CPT invariance, that is Charge conjugation, Parity inversion and Time inversion [8].

CP violation appears on weak interactions on the mixing terms of the charged gauge bosons. Here CP is conserved only if the mixing matrix is real ($V = V^*$). Then measurements of the complex phase δ in the CKM matrix give us a measurement of the amount of CP violation

coming from weak interactions. This can be seen graphically in the unitarity triangle, since if the CKM matrix is real the triangle collapses into a line. Hence the amount of CP violation in the SM can be seen on the measurement of the angles α, β and γ, shown in figure **2-2**.

Physical effects of CP violation are observed by looking at CP conjugate decays of mesons and baryons. Given a decay $M \to f$ with decay amplitude A_f and its CP conjugate $\bar{M} \to \bar{f}$ with decay amplitude $\bar{A}_{\bar{f}}$, the complex parameters of the different terms in the Lagrangian that participate in the decay will appear as phases in the decay of M and its CP conjugate $\bar{M}$. These phases can come from coupling with the charged gauge bosons $W^{\pm}$ or from re-scattering of intermediate states, usually mediated by strong interactions. Hence we can parametrize the decay amplitudes as

$$A_f = \sum_i |a_i| e^{i(\delta_i + \phi_i)}, \tag{2-52}$$

$$\bar{A}_{\bar{f}} = \sum_i |a_i| e^{i(\delta_i - \phi_i)}, \tag{2-53}$$

where $|a_i|$ is the magnitude of the different contributions to the decay amplitude, δ_i and ϕ_i the strong and weak phases respectively. It is assumed that the strong phases δ_i are CP invariant, and therefore do not flip sign under CP. The CP asymmetry is then defined as

$$\mathcal{A}_{CP} = \frac{|A_f|^2 - \left|\bar{A}_{\bar{f}}\right|^2}{|A_f|^2 + \left|\bar{A}_{\bar{f}}\right|^2}. \tag{2-54}$$

Taking as an example the case of a two component amplitude

$$A_f = |a_1| e^{i(\delta_1 + \phi_1)} + |a_2| e^{i(\delta_2 + \phi_2)}, \tag{2-55}$$

$$\bar{A}_{\bar{f}} = |a_i| e^{i(\delta_i - \phi_i)} + |a_i| e^{i(\delta_i - \phi_i)}. \tag{2-56}$$

The CP asymmetry will be

$$\mathcal{A}_{CP} = -\frac{2|a_1 a_2| \sin(\delta_2 - \delta_1) \sin(\phi_2 - \phi_1)}{|a_1|^2 + |a_2|^2 + 2|a_1 a_2| \cos(\delta_2 - \delta_2) \cos(\phi_2 - \phi_1)}. \tag{2-57}$$

It is noted how the asymmetry depends on $\delta_2 - \delta_1 \neq 0$ and $\phi_2 - \phi_1 \neq 0$ to be able to measure a difference in the weak phases. Therefore the presence of interference between two different components with different relative strong phases is needed for the observation of direct CP violation.

Indirect detection of CP violation appears through the study of the decay modes of the neutral meson mixing. For the case of Kaons the quark content of the four possible strange pseudo-scalar mesons is

$$K^+ = (\bar{s}u), \quad K^- = (s\bar{u}), \quad K^0 = (\bar{s}d), \quad \bar{K}^0 = (s\bar{d}). \tag{2-58}$$

In this representation it can be shown that K^0 and $\bar{K}^0$ are CP conjugates of each other, but they are not eigenstates of the weak interaction Hamiltonian. Hence they can mix among each other and the physical states will be given by

$$K_S^0 = \frac{K^0 - \bar{K}^0}{\sqrt{2}}, \tag{2-59}$$

$$K_L^0 = \frac{K^0 + \bar{K}^0}{\sqrt{2}}, \tag{2-60}$$

The short-lived (K_s^0) and long-lived (K_L^0) kaons, the actual mass eigenstates. These two are not anti-particles of each other so they are not required to have same mass and lifetimes. Given that

$$CP\left|K^0\right\rangle = -\left|\bar{K}^0\right\rangle, \;\; CP\left|\bar{K}^0\right\rangle = -\left|K^0\right\rangle. \tag{2-61}$$

Then

$$CP\left|K_S^0\right\rangle = -\left|K_S^0\right\rangle, \;\; CP\left|K_L^0\right\rangle = \left|K_L^0\right\rangle. \tag{2-62}$$

We can observe that K_S^0 is CP even which would allow it to decay into a pair of pions $\pi^{\pm(0)}\pi^{\mp(0)}$, but K_L being CP odd should decay into a 3π final state instead. The first experimental observation of CP violation comes from the measurement of long lived neutral Kaons decaying into a pair of pions [24]. Being the amplitude ratio between these two decays of the order 10^{-3} [3]. Direct CP violation measurements on that same decay channels were performed a few years later [25].

Mixing in the charm sector has been established by different measurements [26–29]. Recently results of direct CP violation have been shown by the LHCb collaboration by measuring the difference between the CP asymmetries on the decay channels $D^0 \to K^-K^+$ and $D^0 \to \pi^-\pi^+$ [2]. Although predictions on the SM parameters are difficult from measurements on charm decays, CPV effects are expected to be very small, so that measurement larger than expected can give us a hint on physics beyond the SM.

In charged $D_{(s)}$ decays, Cabibbo-Suppressed modes are important since other channels might have effects too small to be detected by current experiments. In particular, searches of three and four body final states can show CP violating effects that vary across the phase-space and that can become visible with current data samples.

The B system is where larger CP violating effects have been found in agreement with complex terms appearing in the V_{ub} CKM element at the order of λ^3 [30, 31]. Subsequently observations of direct CP violation in B^0, B^+ and B_s^0 have also been found [32–37]. Model independent analyses have been used to study CP asymmetry on the phase space of B mesons

decaying to three-body final states, showing large effects on specific regions of the Dalitz plot [38] while amplitude analyses for $B^{\pm} \to K^{-}K^{+}\pi^{\pm}$ have shown large CPV effects [39]. At present measurements all these observations seem to be in agreement with SM expected values with some tensions in certain measurements that have not been confirmed and no hints of new physics have been observed [3].

3. Dalitz Plot analysis

In the study of decays of mesons to three pseudo-scalars the common tool to represent the process dynamics is using the Dalitz Plot, where a two dimensional representation of the phase space of the decay is done using the invariant mass of any two pairs of final states (s_{12}, s_{13}, s_{23}). This description comes from the ability to describe the decay amplitude of these types of decay using only two independent degrees of freedom.

This description has been used to study the decay amplitudes of B and D mesons and the resonant structure of their decays, also for the study of CP violation. The description of the amplitudes is usually done using the isobar model, which describes the decay as a coherent sum of intermediate resonant and non-resonant states. Alternative, model independent approaches to study the Dalitz plots, like the Miranda procedure have been proposed for the observation of CP violation and its the subject of our present study.

3.1. Three-body phase space

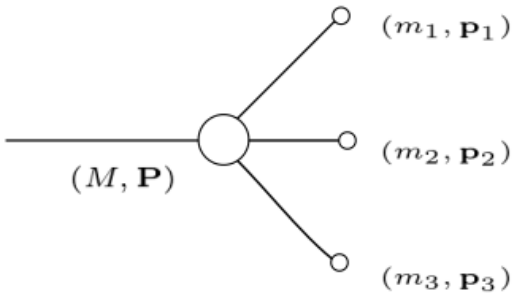

Figure **3-1**.: Scheme of the decay of $1 \to 3$.

The decay rate of a three body decay is described by

$$d\Gamma = (2\pi)^4 \int \frac{d^3p_1}{(2\pi)^3} \int \frac{d^3p_2}{(2\pi)^3} \int \frac{d^3p_3}{(2\pi)^3} \left(\frac{Mm_1m_2m_3}{EE_1E_2E_3} \right) \tag{3-1}$$

$$\times \delta^3(p_1 + p_2 + p_3 - P)\delta(E_1 + E_2 + E_3 - E)|\mathcal{M}|^2, \tag{3-2}$$

where the squared amplitude of the decay $|\mathcal{M}|^2$ describes the dynamics of the process. Simplifications on this decay rate on the mother particle rest frame reduce the decay rate to the expression

$$d\Gamma = \frac{2m_1m_2m_3}{(2\pi)^3(4M^2)} \int ds_{12}ds_{13}|\mathcal{M}|^2, \tag{3-3}$$

with s_{ij} the squared invariant masses for the $i + j$ particles system.

In this description the structure of the decay will be shown by the invariant amplitude $|\mathcal{M}|^2$. If the decay is purely kinematic the amplitude will be constant over the whole phase space, otherwise any dynamical intermediate structure will be shown in the Dalitz plot as density variations across the phase space.

In the center of mass system (cms) the invariant masses are given by,

$$s_{ij} = (p_i^\mu + p_j^\mu)^2 = m_i^2 + m_2^2 - 2E_1E_2 - 2\mathbf{p}_1\mathbf{p}_2 \tag{3-4}$$

$$= (P^\mu + p_k^\mu)^2 = M^2 + m_k^2 - 2ME_k. \tag{3-5}$$

where the invariant masses (s_{12}, s_{13}, s_{23}) depend on the momentum of each decay product and

$$s_{12} + m_{23} + s_{13} = M^2 + m_1^2 + m_2^2 + m_3^2. \tag{3-6}$$

The boundaries of the Dalitz plot will be given by

$$(m_1 + m_2)^2 \leq s_{12} \leq (M - m_3)^2, \tag{3-7}$$

$$(m_1 + m_3)^2 \leq s_{13} \leq (M - m_2)^2, \tag{3-8}$$

$$(m_2 + m_3)^2 \leq s_{23} \leq (M - m_1)^2. \tag{3-9}$$

3.2. Dalitz plots for the analysis of meson decays

The first appearance of a two dimensional diagram for the description of 3-body decays came from the description of what was known as the $\tau^+ \to \pi^+\pi^+\pi^-$ decay mode by Dalitz [4]. This will later be identified as a mode of the charged kaon K^+ where the first observations

of P violation in decays of mesons where reported. There, events obtained for the given decay lie inside an equilateral triangle where the limits of that triangle are given by the kinematical limits of the decay. In the non-relativistic limit events were bounded inside the circle inscribed on the triangle. In figure **3-2** the available phase space for the decays $D^+ \to K^-K^+\pi^+$ and $B^+ \to K^-K^+\pi^+$ is shown.

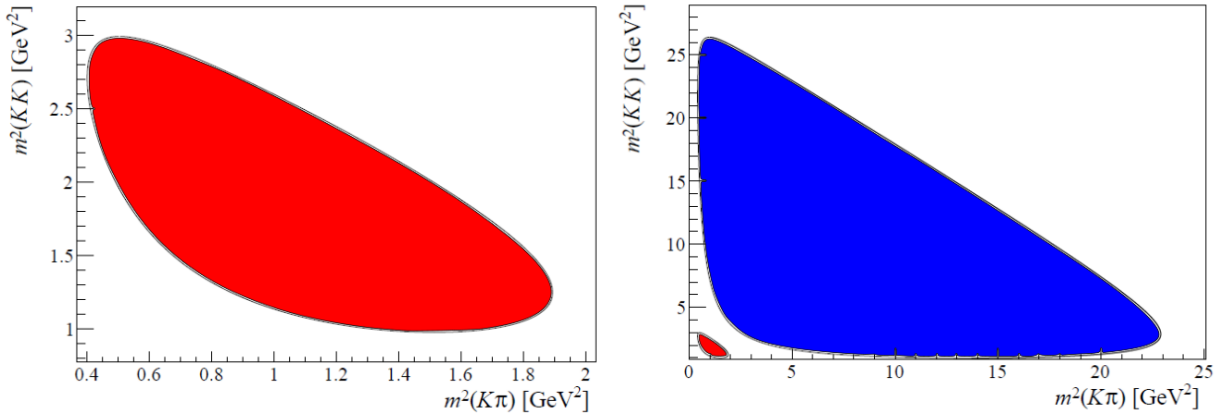

Figure **3-2**.: Comparison of the available phase space for the decays $D^+ \to K^-K^+\pi^+$(left) and $B^+ \to K^-K^+\pi^+$(right).

In recent years, as data samples for decays of B and D mesons has grown. Dalitz Plots have become an standard tool for the study of the dynamical structure of the three final states decays, particularly because they allow for the observation of interference patterns, the extraction of intermediate states of the decay, their spin and the interfering phases which are fundamental for the CP content extraction.

3.3. Amplitude analysis

Description of the amplitude of three body decays is done using intermediate resonances that describe the decay in the form

$$M \to (r \to ab)c. \tag{3-10}$$

The amplitude is modeled as a coherent sum of different resonant states and non-resonant contributions

$$\mathcal{M}(s_{ab}, s_{ac}) = \sum_i a_i e^{i\delta_i} A_i(s_{ab}, s_{ac}) + a_{NR} e^{i\delta_{NR}} f_{NR}(s_{ab}, s_{ac}), \tag{3-11}$$

where a_i and δ_i are the relative magnitudes and relative phases of each component in the amplitude. The dynamical behavior of each resonance is modeled on the amplitude $A_i(s_{ab}, s_{ac})$. For a resonance $r \to ab$ is modeled in the form

$$A(s_{ab}) = B_M^L(pR^M)B_r^L(qR^r)Z_L(\mathbf{p},\mathbf{q})R(s_{ab}). \tag{3-12}$$

$B_M^L(p,p_0)$ and $B_r^L(q,q_0)$ are the penetration factors of the mother particle and the resonance respectively, while $Z_L(\mathbf{p},\mathbf{q})$ is the angular distribution of the final states and $R(s_{ab})$ is the line-shape that describes the resonance. $\mathbf{p}$ is the momentum of the particle that doesn't participates in the resonance, the bachelor ($\mathbf{p}_c$) and $\mathbf{q}$ is the momentum of one of the products of the resonance decay ($\mathbf{p}_a$ or $\mathbf{p}_b$), R^M and R^r are the barrier effective radius for the mother particle and the resonance.

The helicity formalism included in $Z_L(\mathbf{p},\mathbf{q})$ is modeled by the Zemach tensors [40] that describe the angular probability distribution for a resonance with angular momentum L

$$L = 0: \; Z_0(\mathbf{p},\mathbf{q}) = 1, \tag{3-13}$$
$$L = 1: \; Z_1(\mathbf{p},\mathbf{q}) = -2\mathbf{p}\cdot\mathbf{q}, \tag{3-14}$$
$$L = 2: \; Z_2(\mathbf{p},\mathbf{q}) = \frac{4}{3}\left[3(\mathbf{p}\cdot\mathbf{q})^2 - (pq)^2\right], \tag{3-15}$$
$$L = 3: \; Z_3(\mathbf{p},\mathbf{q}) = -\frac{24}{15}\left[5(\mathbf{p}\cdot\mathbf{q})^3 - 3(\mathbf{p}\cdot\mathbf{q})(pq)^2\right]. \tag{3-16}$$

The form factors introduced in the resonance amplitude are the Blatt-Weisskopf barrier factors for the production ($B_M^L(\mathbf{p})$) and decay ($B_r^L(\mathbf{q})$) of resonances of spin L [41]. Considering a barrier radius R, the barrier factors are given by

$$L = 0: \; B^0(z) = 1, \tag{3-17}$$
$$L = 1: \; B^1(z) = \sqrt{\frac{1+z_0^2}{1+z^2}}, \tag{3-18}$$
$$L = 2: \; B^2(z) = \sqrt{\frac{z_0^4+3z_0^2+9}{z^4+3z^2+9}}, \tag{3-19}$$
$$L = 3: \; B^3(z) = \sqrt{\frac{z_0^6+6z_0^4+45z_0^2+225}{z^6+6z^4+45z^2+225}}, \tag{3-20}$$

where $z = pR$, and z_0 is the value of z when $m = m_0$. Finally the lineshape of the resonance is described by the relativistic Breit-Wigner (BW) propagator

$$R(m) \sim \frac{1}{(m-m_0)^2 - im_0\Gamma(m)}, \tag{3-21}$$

for a resonance of mass m_0 and width Γ_0, and

$$\Gamma(m) = \Gamma_0 \left(\frac{q}{q_0}\right)^{2L+1} \left(\frac{m_0}{m}\right) \left[B^L(qR^r)\right]^2, \tag{3-22}$$

being q_0 the value of q at $m = m_0$.

The description of the amplitude as a superposition of Breit-Wigner intermediate states is known to violate unitarity. This effect is increased for broad overlapping resonances. As an alternative the transition matrix of the decay can be described using the K-matrix formalism, which indicates the right approach for including different intermediate states while preserving unitarity [5].

Controversial light scalar states have been found below the $2GeV$ threshold, where the description is hard because of large widths and strongly overlapping states are found that make them difficult to resolve [42]. In this region non-$q\bar{q}$ contributions are expected, like glueballs and multiquark states that would be found below $2GeV$ [43]. For these cases the masses and widths of the resonances are found by poles in the process amplitude (T and S matrices) at the complex energy plane by the form

$$\sqrt{s_{pole}} = m - i\Gamma/2. \tag{3-23}$$

In the case of large width scalar mesons the propagators are described by

$$R(m) = \frac{1}{m_0^2 - m^2 + i\epsilon}. \tag{3-24}$$

In the case where the invariant amplitude of the decay is constant, this will appear as a DP with uniform density of points over the entire space. Information on the intermediate states is observed as variations over the DP. Resonances appear as enhancements on the invariant mass of the decay products of the resonance, as shown in figure **3-3**. In figure **3-4** it can be observed how a wider resonance affects the distribution of points on the DP. The spin of the resonance can also be observed from the number of zeros produced in the decay amplitude as shown in figure **3-5**.

The study of the decay amplitudes of meson decays is usually done by performing likelihood fits that include different contributions of resonant and non-resonant terms across the phase space of the decay that allow for a precise description of the amplitude. Other approaches for the study of CP violation in three-body decays that aim for a model independence rely on observation of the asymmetries across the phase space of the decay.

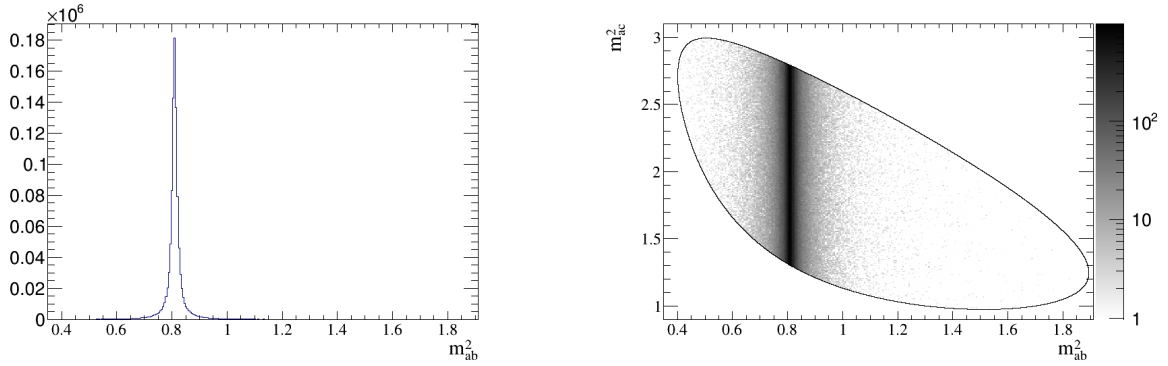

Figure **3-3**.: Dalitz Plot and lineshape described by a single Breitt-Wigner resonance.

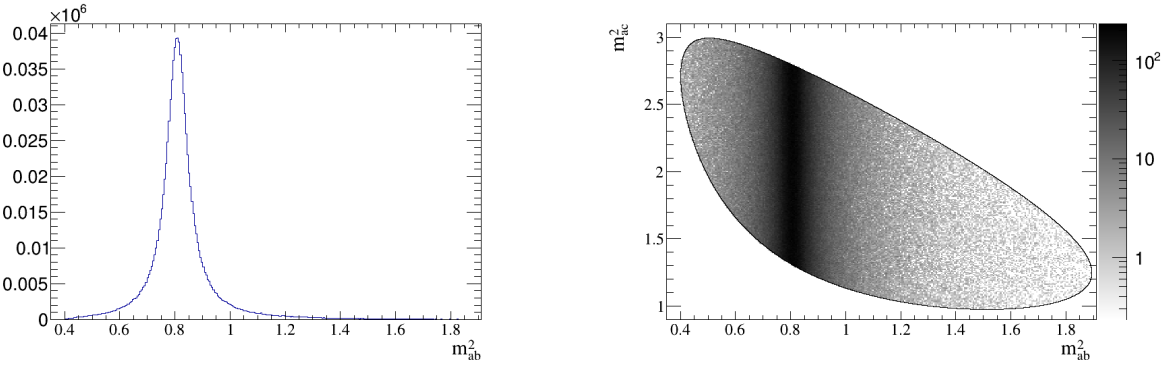

Figure **3-4**.: Dalitz Plot and lineshape described by a single Breitt-Wigner resonance with a larger width.

3.4. Miranda procedure

As available data samples for decays of heavy mesons become larger more interests is addressed towards the three-body decays of B and D mesons. A model independent way of measuring CP violation in these decays would be to do a direct comparison of the binned DP between CP conjugate decays. As shown in section 2.4 direct CP violation in decays can be measured by computing the asymmetry between the square of the decay amplitudes, in binned DP these amplitudes are observed as number of events at each bin $N(i)$ for the particle and $\bar{N}(i)$ for its antiparticle. Hence the asymmetry of a bin i in the Dalitz plot will be defined as

$$A_{CP}(i) = \frac{N(i) - \bar{N}(i)}{N(i) + \bar{N}(i)}. \tag{3-25}$$

The use of the asymmetry $A_{CP}(i)$ for the detection of CP violation in a binned analysis makes the study more sensible to statistical fluctuations [6,7]. Instead it is proposed the use

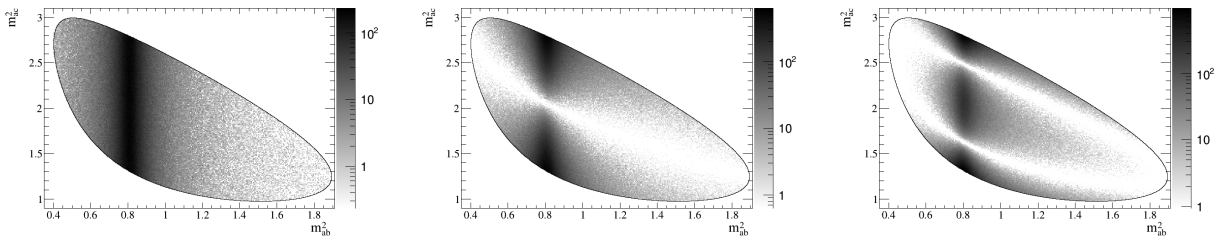

Figure **3-5**.: Dalitz Plot obtained by a resonance with spin 0 (left), 1(center) and 2(right).

of the significance

$$S_{CP}(i) = \frac{N(i) - \alpha\bar{N}(i)}{\sqrt{\alpha(N(i) + \bar{N}(i))}}, \tag{3-26}$$

with the normalization factor $\alpha = N/\bar{N}$, here $N(\bar{N})$ are the total number of events for the particle (anti-particle) decay. The significance values will be calculated bin-by-bin and for the case where no CP asymmetry exists in the sample, S_{CP} should distribute as a Gaussian with $\mu = 0$ and $\sigma = 1$. In that case significant deviations from that behavior will be interpreted as evidence for CPV [44].

As was shown in section 2.4, for a direct observation of CPV, the interference of weak and a strong phases is needed. These complex phases only become observable as relative phases in the interference of two decay channels. Hence for this analysis the focus of interest will be in the region of intersection of the main resonances of the decay. Since this is the region where CPV observation is possible and the region that has a higher statistics in the phase space. To account for these local asymmetries is important to choose a binning scheme across the Dalitz plot that allows for the observation of such effects. An adaptive binning scheme where bins are defined in a way that all bins have the same number of events is also performed, this analysis is presented in chapter 4.

3.5. Charmed mesons to three-body final states

Decays of heavy mesons are usually defined depending on the degree of suppression by the CKM matrix elements involved in the process, being the elements on the diagonal Cabbibo Favoured (CF), changes from one family to the next are Cabbibo Suppressed (CS) while changes between the first and third quark family are Doubly Cabibbo Supressed (DCS).

The main diagram through which the decay $D^+ \to K^-K^+\pi^+$ occurs at tree level is CS for it occurs at elementary level by the process $c \to du\bar{d}$ or $c \to su\bar{s}$. Tree level diagram of this

process is shown in figure **3-6**a, at higher orders this can also occur through the "penguin" diagram shown in figure **3-6**b. The different components of the intermediate resonant $q\bar{q}$ states by which this decay goes from 1 to 3 bodies is what give us the characteristic dynamics shown in the Dalitz plot that are shown in the invariant mass of the K^-K^+ and $K^-\pi^+$ pairs. The contribution of each of these diagrams come into the decay amplitude as the components of a coherent sum of amplitudes, as described in 3-11.

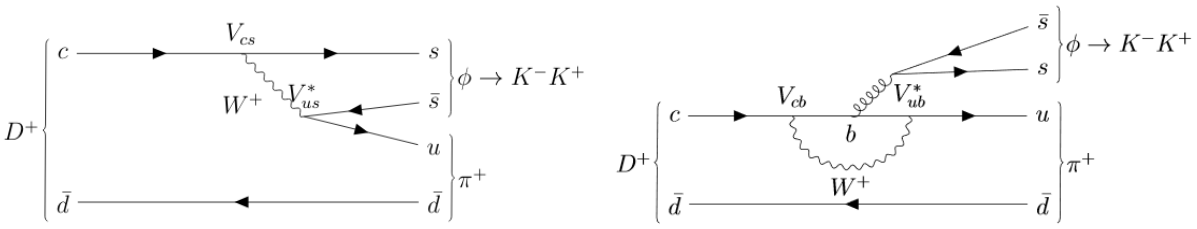

Figure **3-6**.: Example Feynamn diagrams that participate in the Cabibbo suppressed decay of the D^+ meson. Tree level (left) and penguin diagram (right).

As can be noted in equation 2-42, the CKM matrix elements that participate in these decays have an imaginary part at the order of $Im(V_{cd}) \sim \lambda^5$ at the three level and $Im(V_{ub}) \sim \lambda^3$ in the penguin diagram, which is loop suppressed, in the Wolfenstein parametrization. The CPV effects that may be observed on decays of charmed mesons are expected to be very small in contrast with B meson decays where asymmetry effects apper at the order of λ^3. This makes the study of CP violation in decays of charm mesons of particular interest as an asymmetry larger than expected would be a hint towards new physics.

4. The LHCb experiment

The LHCb detector [45,46] is a single-arm forward spectrometer covering the pseudorapidity range $2 < \eta < 5$, designed for the study of particles containing b or c quarks. The detector includes a high-precision tracking system consisting of a silicon-strip vertex detector surrounding the pp interaction region [47], a large-area silicon-strip detector located upstream of a dipole magnet with a bending power of about $4Tm$, and three stations of silicon-strip detectors and straw drift tubes [48] placed downstream of the magnet. The tracking system provides a measurement of the momentum, p, of charged particles with a relative uncertainty that varies from 0.5% at low momentum to 1.0% at $200GeV/c$. The minimum distance of a track to a primary vertex (PV), the impact parameter (IP), is measured with a resolution of $(15 + 29/pT)\mu m$, where p_T is the component of the momentum transverse to the beam, in GeV/c. Different types of charged hadrons are distinguished using information from two ring-imaging Cherenkov detectors [49]. Photons, electrons and hadrons are identified by a calorimeter system consisting of scintillating-pad and preshower detectors, an electromagnetic and a hadronic calorimeter. Muons are identified by a system composed of alternating layers of iron and multiwire proportional chambers [50]. The online event selection is performed by a trigger [51], which consists of a hardware stage, based on information from the calorimeter and muon systems, followed by a software stage, which applies a full event reconstruction.

4.0.1. Detector layout

The LHCb spectrometer is build in the forward region with an angular coverage from $10mrad$ to $300mrad$ in the bending plane and $250mrad$ in the non-bending plane. This layout was chosen because $b\bar{b}$ pairs coming from pp collision on the LHC are produced mostly in the same forward and backward cone. A view of the LHCb detector is shown in figure **4-1**.

A warm dipole magnet of an integrated magnetic field of $4Tm$ with saddle shaped coils in a window frame yoke is used on the detector. Each coil is arranged in five triplets of pancakes-shaped with an specific ohmic resistance below 28Ω at $20°$.

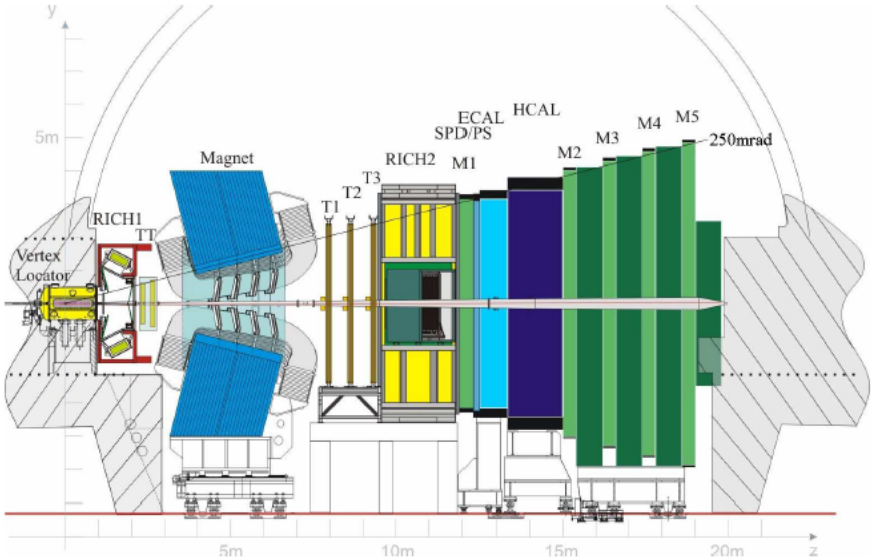

Figure **4-1**.: The LHCb detector. Taken from [45].

4.0.2. Tracking

The tracking system consists of the vertex locator system (VELO), the tracking stations Tracking Turicensis (TT) that are made of silicon micro strip detectors placed upstream from the magnet, and three tracking stations (T1-T3) made of silicon microstrips in the inner region (IT) and straw tubes in the outer region (OT) placed downstream of the magnet.

Vertex Locator (VELO)

The VELO system measures the track coordinates close to the interaction used to identify displaced secondary vertices. Is composed of a series of silicon modules that measure r and ϕ polar coordinates along the beam direction. Track coordinates measured by the VELO are used to reconstruct production and decay vertices of b and c hadrons for measuring decay lifetimes and impact parameters for flavour tagging.

Silicon Tracker

The TT and IT stations are made of silicon microstrip sensors. Each station has four layers with vertical strips arranged for the first and last layer and strips rotated by an angle $-5°$ and $+5°$ for the second and third layer. TT modules are arranged in two pairs separated by

$27cm$ along the beam axis. Each IT station is composed of four detector boxes, where each box contains four layers of seven detector modules. Detector modules consist of a single silicon strip and a readout hybrid.

Outer Tracker

The OT is a drift-time detector for the tracking and measurement of the momentum of charged particles. The detector is composed of an array of individual, gas-tight straw-tube modules. There are two layers of staggered drift-tubes. Each station is composed of four layers in the same geometry as in the IT modules for the three tracking stations (T1-T3).

4.0.3. Particle identification

A key feature of the LHCb detector is its ability to distinguish clearly pions and kaons, this is done by an efficient particle identification system. For this task two Ring Imaging Cherenkov (RICH) detectors, a system of Electromagnetic and Hadron Calorimeters and a set of Muon chambers are used.

RICH

Two RICH detectors are placed to cover the full momentum range of charged particles. RICH 1 is located upstream from the magnet between the VELO and the TT stations and is designed to cover the low momentum range from $1GeV/c$ to approximately $60GeV/c$ using aerogel and C_4F_{10} radiators. RICH 2 is located downstream from the magnet between the last tracking station and the first muon chamber. and covers the high momentum range from $15GeV/c$ up to more than $100GeV/c$ using a CF_4 radiator. For both detectors Cherenkov light is focused using spherical and flat mirrors to reflect the light out of the detector acceptance into the hybrid photon detectors. The photon detectors are surrounded by external magnetic shields.

Calorimeters

The calorimeter system is designed for the selection of transverse energy in hadron, electron and photon candidates for the first level trigger and the reconstruction of π^0 and prompt photons that are essential for flavour tagging. The structure consist of an electromagnetic

calorimeter (ECAL) followed by a hadron calorimeter (HCAL). For the rejection of a high background of charged pions a pre-shower detector (PS) is used upstream from the ECAL, high background π^0's are rejected using a scintillator pad detector (SPD) to select charged particles.

Muon stations

Muon triggering and identification is fundamental as muons are present in the final state of many CP-sensitive decays. The muon system provides information for the high p_T muon trigger at the Level-0 trigger and muon identification for the High Level Trigger. The detector is composed of five rectangular stations. The first, M1 is placed upstream from the calorimeters and is used to improve measurements on p_T for the trigger. M2-M5 are placed downstream from the calorimeters separated by $80cm$ thick iron absorbers. Minimum momentum for a muon to cross all the stations is around $6GeV/c$. The detectors space point measurements of the tracks in the form of binary information to the trigger. Alignment of the hits in all five stations is required for the muon trigger.

4.0.4. Trigger

LHCb trigger is composed of two levels, Level-0 (L0) trigger operates synchronously with the bunch crossing frequency while the High Level Trigger (HLT) operates asynchronously on a processor farm.

Level-0 trigger (L0)

L0 trigger attempts to reconstruct the highest E_T hadron, electron and photon clusters in the calorimeters and the two highest p_T muons. From the pile-up system in the VELO the number of primary pp interactions in each bunch is estimated, with calorimeter information the total observed energy and the number of tracks is estimated based on the SPD hits. Based on the information obtained, events may be rejected to avoid large occupation on the HLT data-flow. The complete L0 trigger information is collected by the Decision Unit (DU) and makes a final decision for each bunch crossing.

L0 information is composed of three parts, pile-up system, L0 calorimeter trigger and L0 muon trigger. The DU collects all the information for the evaluation of the final decision. The Pile-up system provides information on the position of the primary vertices and the

backward charged track multiplicity. Calorimeter trigger looks for high E_T clusters an identifies them based on information from the SPD, PS, ECAL and HCAL detectors. Muon chambers allow the muon reconstruction selecting the two muons with highest p_T for each quadrant of the detector.

High Level Trigger (HLT)

HLT is a *C++* application running on every CPU of the Event Filter Farm (EFF) that contains up to 2000 computing nodes. It access to all available data from the detector for one event. Is composed of two stages, HLT1 and HLT2. At HLT1 the reconstruction of particles in the VELO and T-stations is done from the L0 information. HLT2 combines all the information and trigger algorithms to fully reconstruct the final states.

5. CP violation on the decay $D^+ \to K^-K^+\pi^+$ at the LHCb experiment

The Cabibbo suppressed decay $D^+ \to K^-K^+\pi^+$ is of interest for the study of CP violation in decays of charm mesons at the LHCb collaboration, where an analysis has already been performed using the Miranda procedure on the Run I data set of year 2010. For the Run II a larger data sample is expected. A sensitivity study for the detection of CP violation on the decay $D^+ \to K^-K^+\pi^+$, using the Miranda procedure, within the LHCb Run II data size, is proposed on Monte Carlo generated samples. Where asymmetries are introduced via relative differences on the decay amplitude of different components of the model used for their study between the D^+ and D^- data sets.

These studies on the decay channel of interest aim to have a description of the level of CP asymmetry that we would be able to measure with a given data set size with a certain purity of the sample. For this, a toy Monte Carlo model is constructed using the *Laura++* package [52]. This is a set of *C++* based libraries constructed on the *ROOT CERN* data analysis framework [53] for fitting and generating samples of a given decay amplitude of $1 \to 3$ body decays. For our sensitivity studies we are interested in constructing a model for the lineshape spectrum of the decay mode that reproduce as much as possible the dynamics of the real decay. This includes a model for intermediate states resonances, and a simple background model. Different samples with some amount of CP asymmetry are generated along the main resonances of the decay and the Miranda procedure is performed on them. A sensitivity study can also indicate to us the most sensitive binning strategy for the detection of a CP violating signal in a given region of the Dalitz plot. Here three possible binning schemes are studied. An uniform binning with equal size square bins distributed along the DP phase space. An adaptive binning where rectangular bins are defined so that there is approximately the same number of events for the sum of the events on both charmed meson charges and a physics motivated binning, where bins are defined paying special attention to the regions on the main resonances of the decay an the structure on each side.

Previous analysis on this decay channel have been performed with samples of $\sim 2 \times 10^5$ by the CLEO collaboration [54] and the most recent analysis using the Miranda procedure by the LHCb collaboration on Run I data taken during the year 2010 of $\sim 4 \times 10^5$ events with no observable CPV asymmetry found [44]. For the Run II a larger data set is expected. With a total integrated luminosity of $\mathcal{L} = 5.67 fb^{-1}$ for the years $2016 - 2018$ and a charm production cross section of $\sigma(pp \to D^+X) = 834 \pm 2 \pm 78 \mu b$ on the LHCb acceptance at a center of mass energy of $\sqrt{s} = 13TeV$. This will account for a production of $\sim 4.7 \times 10^{12}$ $D^\pm$ events. After selection it is expected to have a data set of roughly 2×10^8 events of $D^+ \to K^-K^+\pi^+$ with $\sim 90\%$ purity, this is the data size we will aim to study in our Monte Carlo generation.

A short discussion on the proposed data selection for the Run II available data and finally a study of the Miranda procedure applied to the sidebands of the $D^\pm$ invariant mass data sets for the verification of existent CPV signals coming from the background is also shown. For the analysis on the decay mode $D^+ \to K^-K^+\pi^+$, the decay $D_s^+ \to K^-K^+\pi^+$ is selected as control mode as is has the same final state structure and no observable CPV asymmetry is expected to be observed in this channel. Hence, a data selection that controls all production asymmetries on the D_s^+ mode will ensure that any asymmetry that may be found on the D^+ decay will be due to CPV effects by applying the same data selection on both cases.

5.1. Monte-Carlo generation

The construction of the amplitude model is done according to the isobar model described by the results obtained by the CLEO collaboration [54]. Such a model requires the description of the intermediate states using a magnitude and a relative phase, as given by the isobar model. The amplitudes and phases used are shown in table 5.1.

Resonance	Magnitude	Phase (°)	Fit Fraction (%)
$K^*(892)$	1	0	25.7
$K_0^*(1430)^0$	4.56	70	18.8
$\phi(1020)$	1.166	163	27.8
$a_0(1450)^0$	1.50	116	4.6
$\phi(1680)$	1.86	-112	0.51
$\bar{K}_2^*(1430)^0$	7.6	171	1.7
$\kappa(800)$	2.30	-87	7.0

Table **5-1**.: CLEO model B used for the generation of MC samples of the decay $D^+ \to K^+K^-\pi^+$ [54].

The main resonances of interest are the ones whose fit fraction is greater and are the ones on which we will focus for our studies, these are $K^*(892)$ that decays into a $K\pi$ pair and $\phi(1020)$ that decays into a KK final state. In particular, for this model the $K^*(892)$ is used as reference (magnitude 1 and phase 0°). All the resonant states are defined using a relativistic Breit-Wigner propagator except for the scalar $\kappa(800)$ in which a pole like function was used.

The model used for this initial generation does not include a background component. The following studies will only look at the behavior of the Dalitz Plot on the signal region. Sensitivity studies with the inclusion of a background component in the amplitude model are shown in section 5.7.

5.2. Line shape definition

As shown in previous section we use only 7 intermediate states components to describe the decay amplitude in our Monte-Carlo pseudo-experiment, based on the results obtained by the CLEO collaboration. For the generation process of the entire amplitude care must be taken so that the parameters used by the *Laura++* package are the ones that best describe the expected lineshape of the data. In order to obtain the complete model described in table 5.1 we start by exploring the behavior of the resonant states.

5.2.1. $K^*(892)$

The intermediate state $K^*(892)$ is the main contribution on the invariant mass of the $K\pi$ channel. With a mass of $895.55MeV$, a width of $46.2MeV$ and spin 1, all values of mass and width for the resonance states used are taken from [3]. In the model for the lineshape studied here the $K^*(892)$ resonance is used as reference, is introduced in the model with magnitude 1 and phase 0°. A single component generation of the decay amplitude with the $K^*(892)$ is shown in figure **5-1**.

Here the shape of the BW propagator used to define the amplitude of the resonance can be distinguished on the $K\pi$ system invariant mass. The effect of the vector nature of this resonance can also be seen in the node that appears on the DP and how its reflected along the KK invariant mass.

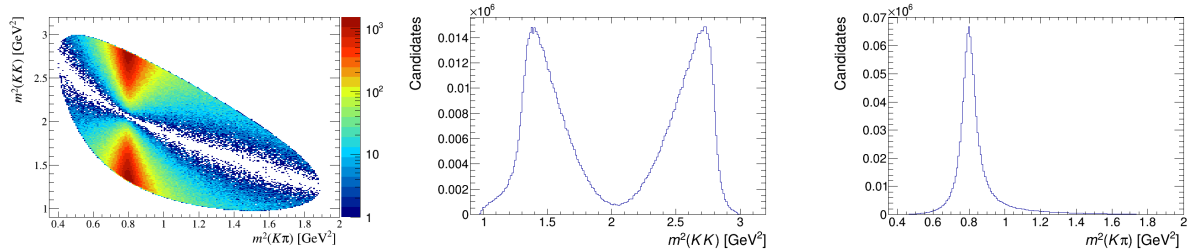

Figure **5-1**.: Dalitz plot of the generated sample including only the $K^*(892)$ component and their projections on the KK and $K\pi$ invariant masses.

5.2.2. $\phi(1020)$

The other important contribution to the decay amplitude of the process of interest is the $\phi(1020)$ intermediate state that goes into a pair of kaons KK. For this resonance a mass of $1019.461 MeV$ is used and a width of $4.249 MeV$ with spin 1. Generation of a single component amplitude including the $\phi(1020)$ only is shown in figure **5-2**.

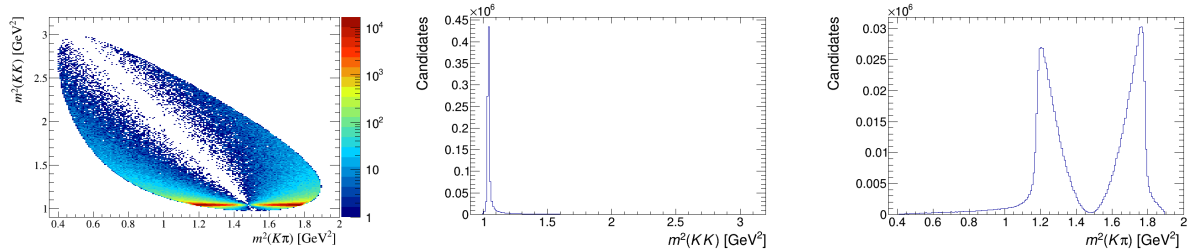

Figure **5-2**.: Dalitz plot of the generated sample including only the $\phi(1020)$ component and the projections on the KK and $K\pi$ invariant masses.

For this case the very narrow shape of the $\phi(1020)$ state is shown on the invariant mass of the KK system. While along the $K\pi$ system the node produced as an effect of its spin is shown as a projection along the $K\pi$ invariant mass.

Considering now the combined amplitude of the $K^*(892)$ and the $\phi(1020)$ components. We perform variations on the relative phase between these two contributions. Here a change can be observed in the distribution of events in the Dalitz Plot, particularly on the region where the two resonances interfere. A comparison of these for different phases of the $\phi(1020)$ contribution is shown in figure **5-3**. It can be seen that as the phase is changed the number of events of different regions of the DP change. Particularly how when the two resonances are on the same phase the constructive interference on the region where they meet is minimum while when the phase difference is 180° the interference is maximal and the region of intersection

has a greater number of events. For the model proposed here we have a relative phase of 163° on the ϕ so we expect a considerable contribution from that region.

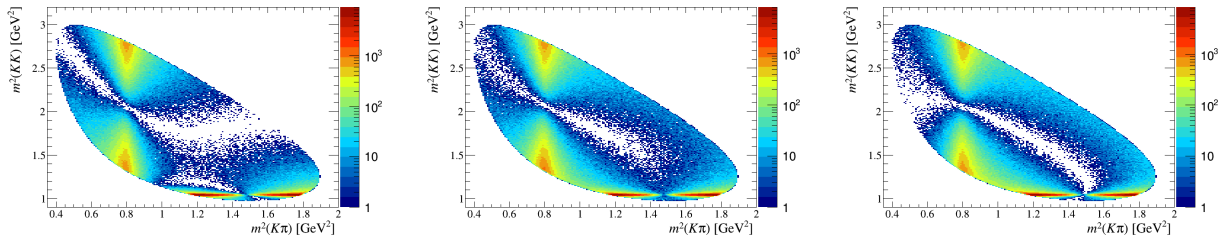

Figure **5-3**.: DP of a sample including the $K^*(892)$ and $\phi(1020)$ changing the relative phase of the ϕ resonance as 0° (left), 90° (center), 180°(right).

Finally the ϕ amplitude is introduced with the 163° phase difference as proposed by the model. The DP and its projections are shown on figure **5-4**.

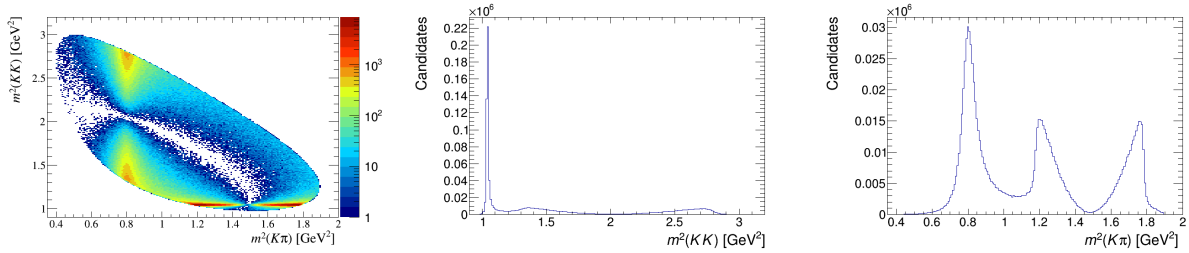

Figure **5-4**.: DP for the generated sample including the main components $K^*(892)$ and $\phi(1020)$ with the parameters proposed by the CELO model.

5.2.3. Other contributions

The combination of the K^* and the ϕ introduced in previous section already defines the larger part of the decay amplitude as defined by the model shown in table 5.1. In the following we show the contribution of the other smaller resonances included in the model towards the final lineshape of the DP. In figure **5-5** the invariant mass projections are shown comparing models where different resonances are included sequentially to the 2 component model in the following order; $K^*(1430) + a_0(1450) + K^{*2}(1430) + \phi(1680)$.

Finally the last part of the $K\pi$ amplitude is introduced using a pole function. The scalar κ contribution to the model used has a mass of $797MeV$ and a width of $410MeV$ that

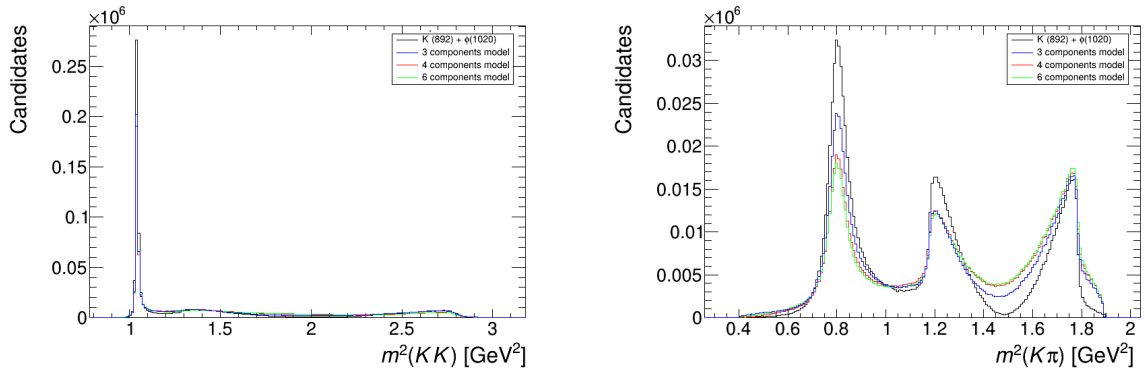

Figure **5-5**.: Invariant mass projections for different models including the components of the CLEO model.

corresponds to the real and imaginary parts of the pole function description whose pole description in the complex plane has the form

$$T_{pole}(m, m_\kappa, \Gamma) = \frac{1}{(m_\kappa + i\Gamma)^2 - m^2} \tag{5-1}$$

Resulting projections of including the κ state are shown in figure **5-6**. Dalitz Plot of the resulting phase space of the complete amplitude model is shown in figure **5-7**.

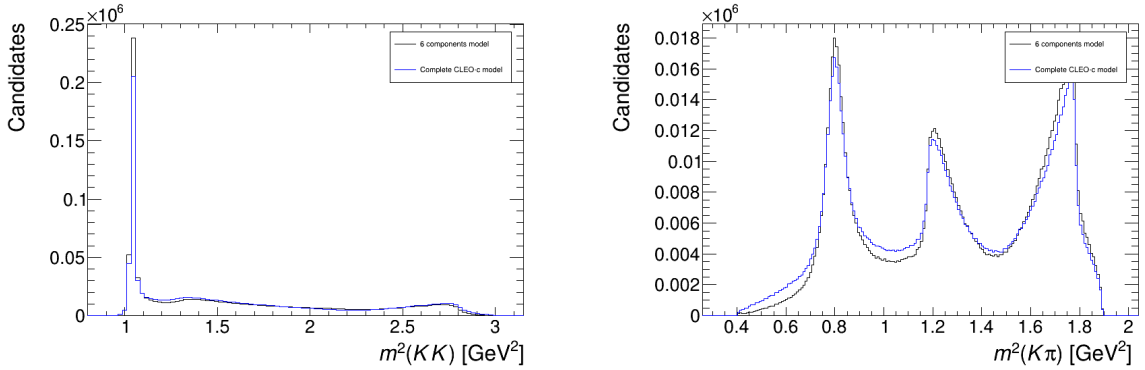

Figure **5-6**.: Invariant mass projections for different models including the 6 components of the CLEO model and finally the complete model that includes the κ pole function.

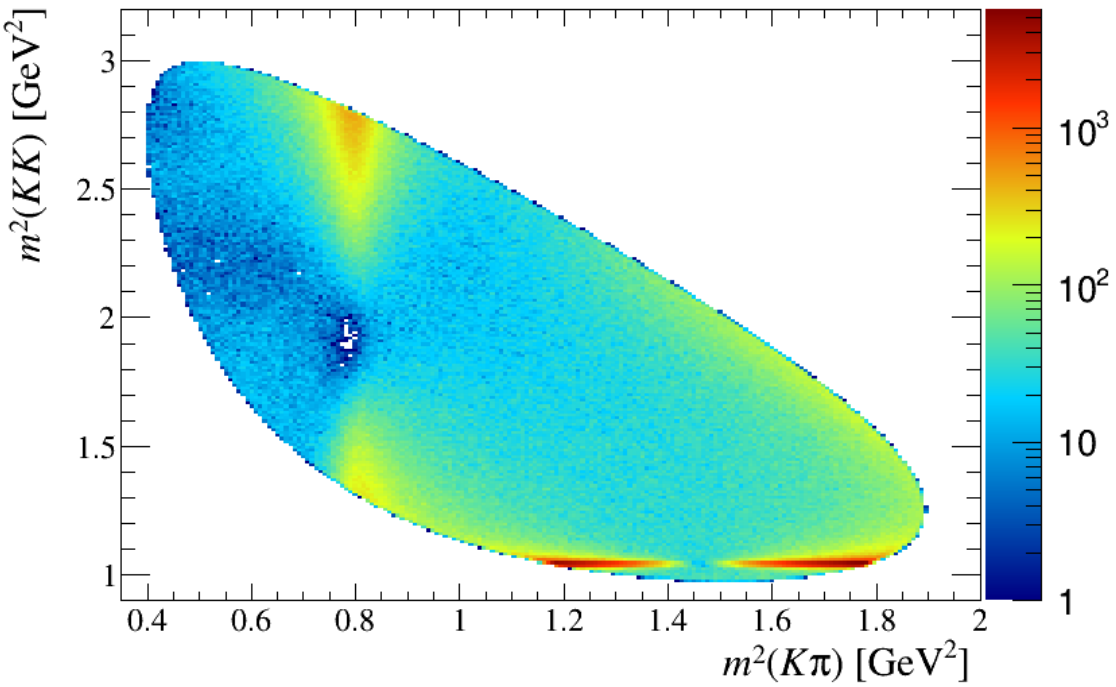

Figure **5-7**.: Dalitz Plot of the final model generated using Laura++ and the CLEO model including 1×10^6 events.

5.3. Initial studies

A first approach towards our sensitivity studies is performing the Miranda procedure on samples with a relatively small number of events (2×10^7 events). In these samples a particular level of asymmetry between the D^+ and the D^- samples is introduced as a shift in the amplitude or the phase of a given resonance. Here we introduce the asymmetry on the $K^*(892)$ and $\phi(1020)$ intermediate states since those are the regions of the DP with greater statistics and from where a visible CP violating signal will be more likely to be detected. Miranda procedure analysis is performed on these samples for a 10×10 uniform binning scheme. Results are shown in table **5-2**.

For each of these samples the S_{CP} observable was calculated bin by bin. In the no-asymmetry case those values should be distributed as a mean 0 and standard deviation 1 Gaussian. As shown in figure **5-8** for the null test, in which no asymmetry is introduced on the amplitude parameters.

It can be seen that the deviation from the expected Gaussian distribution is very low and the

$\Delta a(\%)$	χ^2/ndof	p-value(%)	$\Delta\delta(^\circ)$	χ^2/ndof	p-value(%)
0	60.58/68	72.68	0	60.58/68	72.68
0.1	66.73/68	52.09	0.1	59.66/68	75.47
0.2	78.82/68	17.39	0.2	63.06/68	64.67
0.3	95.08/68	1.68	0.3	70.82/68	38.37
0.4	117.78/68	0.02	0.4	83.50/68	9.75
0.5	144.05/68	2.16×10^{-5}	0.5	99.82/68	0.72
0.6	176.28/68	1.49×10^{-9}	0.6	123.16/68	4.87×10^{-03}
0.7	212.42/68	9.08×10^{-15}	0.7	148.32/68	6.57×10^{-06}
0.8	256.35/68	1.21×10^{-21}	0.8	178.58/68	7.17×10^{-10}
0.9	303.57/68	1.69×10^{-29}	0.9	210.42/68	1.81×10^{-14}
1	355.71/68	1.45×10^{-38}	1	251.08/68	8.53×10^{-21}

Table **5-2**.: Results for 2×10^7 events samples (D^+, D^-) on different asymmetry levels using a 10×10 uniform binning.

values of S_{CP} are between -3 and 3. In figure **5-9** results for some samples where asymmetry is introduced on the relative magnitude of the $K^*(892)$ are shown. Results for asymmetry introduced on the relative phase are shown in figure **5-10**.

The p-value calculated is the probability of obtaining a result as extreme as the observation given that the null test is accepted that is given that no CP violation is present on the decay. Under this scope the statistical significance of such a measurement is obtained from the p-value. If $p \leq 3 \times 10^{-7}$ we would get a statistical significance of 5σ which is the level of significance we would want to pursue. 3σ confidence level is obtained at $p \leq 10^{-3}$.

The obtained results for S_{CP} for these samples will be used as a reference on the level of asymmetry that we will be able to measure on the complete statistics tests. There we expect to measure asymmetries bellow 0.5% of difference in amplitudes and below the 0.5° on the phase differences.

The second binning scheme that will be applied in our studies is an adaptive binning, where a configuration of bins is defined such that the number of events in each bin is to be equal. This is done using the *kdTreeBinning* class of the ROOT framework.

As a test on the behavior of the method a study on the no-asymmetry samples is done using different number of bins as shown in figure **5-11**. Where the number of events in each bin is displayed. It can be seen that as the number of bins increase there is a greater concentration of events near the K^* and particularly on the ϕ resonances. Which are the regions of the DP with a greater density of events as expected. For the proposed Miranda study this is

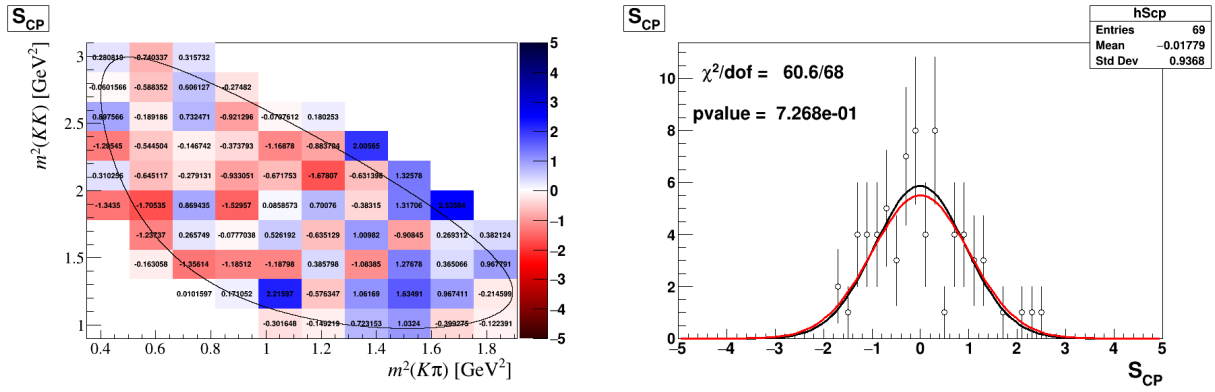

Figure **5-8**.: DP of the Miranda procedure on a 2×10^7 events sample with no introduced asymmetry. On the right is the distribution of the S_{CP} values, black line is the fitted Gaussian distribution and red line is the reference mean 0 and standard deviation 1 Gaussian.

particularly useful because it may increase the sensitivity to CP detection near the regions of interest.

The third binning strategy is to define a grid of rectangular bins in which not only we would want to get bins with very similar number of events but with a closer emphasis on the inner structure of the DP, showing the different regions that the main resonances populate. A 22 bins scheme is used in which the regions of the $K^*(892)$ and the $\phi(1020)$ resonances are divided in four bins each, breaking each resonance into its two peaks and along its mass, a scheme of the bin structure used is shown in figure **5-12**.

5.4. Studies on the number of bins

The asymmetry signal that may be detected from the Miranda procedure is very sensitive to the binning configuration used across the DP, not only on the number of bins used, which will determine the number of degrees of freedom on the χ^2 measurement, but also in their shape. Since different sources of asymmetry may produce different S_{CP} distributions on the phase space particularly near the regions of more interest ($K^*(892)$ and $\phi(1020)$ regions) an adaptive binning scheme is used, where the bins are designed so that each bin on the diagram has approximately the same number of events. A physics motivated binning scheme is also proposed that is designed to take into account the dynamical structure of the DP near the larger resonances.

Considering the uniform binning as a starting point, the behavior of the S_{CP} plots is studied

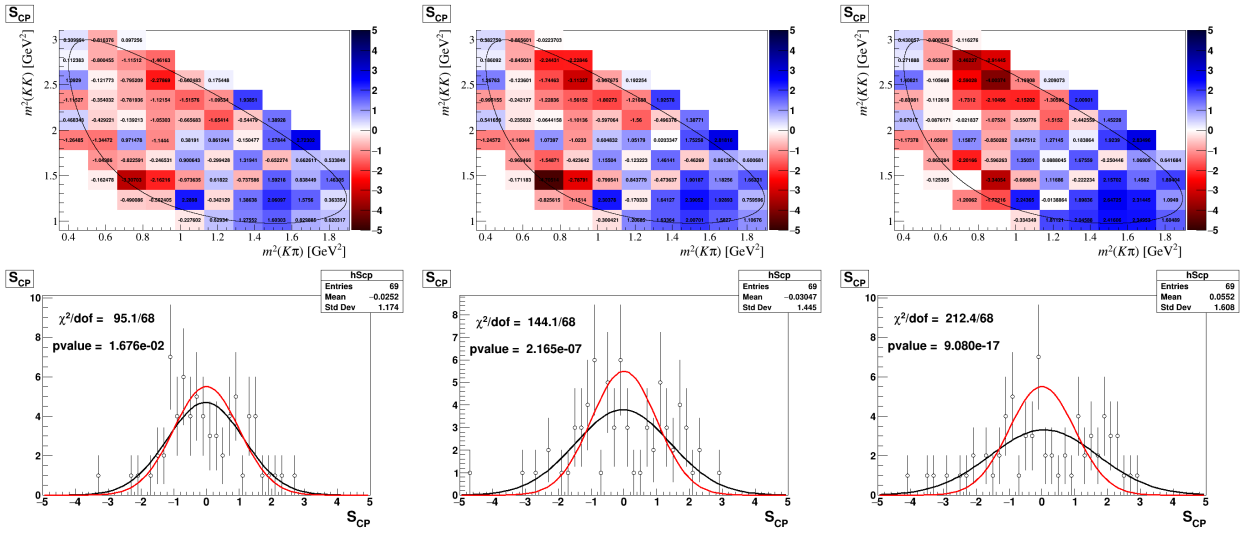

Figure **5-9**.: Results of Miranda procedure applied on samples with different levels of asymmetry along the $K^*(892)$ magnitude. $\Delta a = 0.3\%$(left), $\Delta a = 0.5\%$(center) and $\Delta a = 0.7\%$(right)

under different number of bins for sets of 10 samples generated with introduced asymmetries of $\Delta a = 0.15\%$ and of $\Delta\delta = 0.2°$ on the K^*. Results of the number of samples on which 5σ CPV observation out of 10 are shown in table **5-3**. Some of the S_{CP} plots obtained are shown in figure **5-13**. It can be seen that as the bin size becomes increasingly large the sensitivity to the dynamical structure is reduced, while at small bin size the asymmetry effects tend to be averaged away with the increase on the number of degrees of freedom.

nbins	5×5	7×7	10×10	15×15	20×20
$\Delta a = 0.15\%$	7/10	6/10	4/10	0/10	0/10
$\Delta\delta = 0.2°$	3/10	9/10	5/10	3/10	2/10

Table **5-3**.: Number of samples with observed CPV with a significance of 5σ for samples of introduced asymmetry of $\Delta a = 0.15\%$ and of $\Delta\delta = 0.2°$ on the $K^*(892)$.

In the present analysis we use a χ^2-test for looking at deviations of the S_{CP} distribution from its null-hypothesis. Being the null-hypothesis that no CPV is found. Then, the calculated p-values will be the probability of obtaining such a extreme result given that the null-hypothesis is true (there is no CP violation in the decay channel). In such a case for obtaining an observation of CPV at the 5σ level of confidence it would be necessary to obtain $p-\text{value} \leq 3\times10^{-7}$.

The Z-value distribution is used for obtaining the statistical significance $Z = (x-\mu)/\sigma$ from

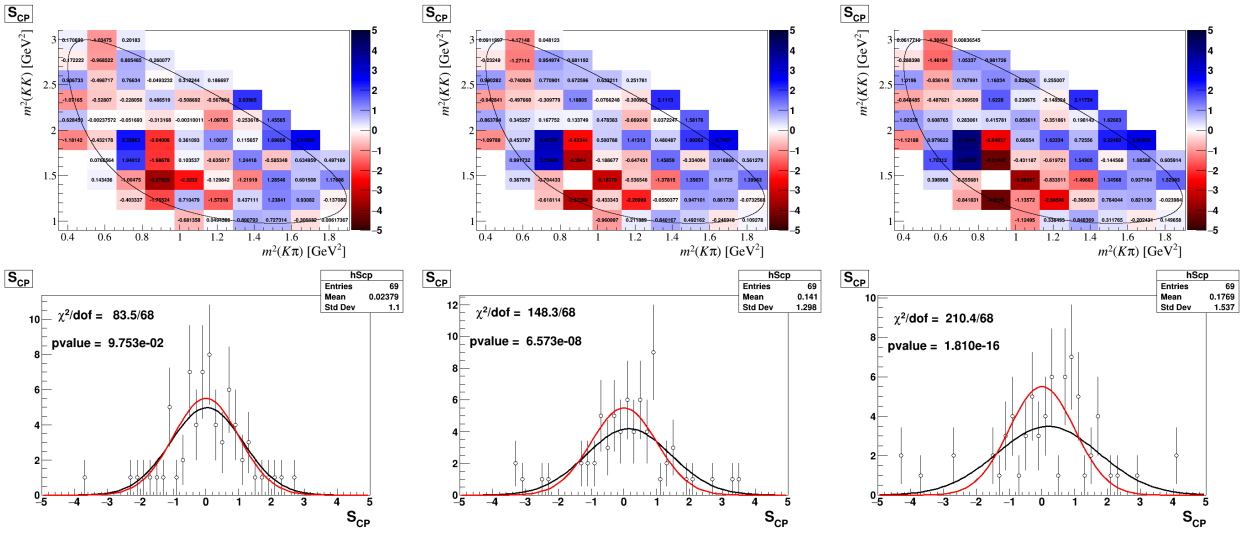

Figure **5-10**.: Results of Miranda procedure applied on samples with different levels of asymmetry along the $K^*(892)$ relative phase. $\Delta\delta = 0.4°$(left), $\Delta\delta = 0.7°$(center) and $\Delta\delta = 0.9°$(right)

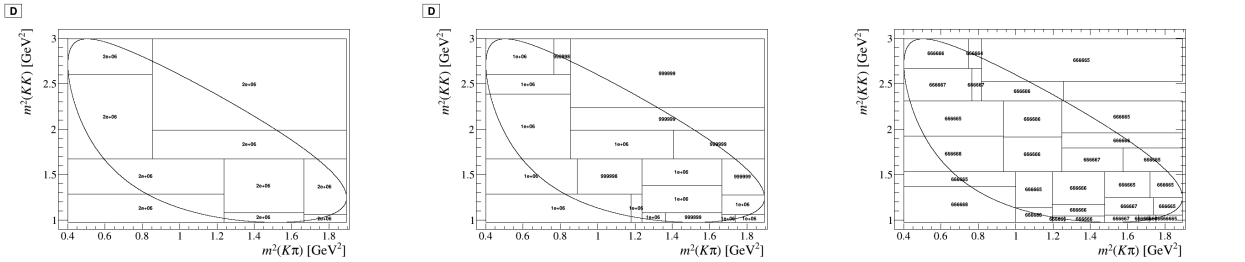

Figure **5-11**.: Configuration of bins using the adaptive binning scheme with 10 bins (left), 20 bins (center) and 30 bins (right).

the obtained p-value by the function

$$Z = \sqrt{2}Erf^{-1}(1-2p), \tag{5-2}$$

where $Erf^{-1}(x)$ is the inverse error function [55].

Results of the $Z - value$ or standard score obtained for all the samples in the different number of bins cases are shown in figure **5-14**. it is clear how in the case of phase difference the 5×5 binning gives a lesser statistical significance than the 7×7 case.

Looking into the adaptive binning, if we analyze the sensitivity of the method with varying number of bins we obtain the results shown on table **5-4**. S_{CP} graphs for some samples are shown in figure **5-15**.

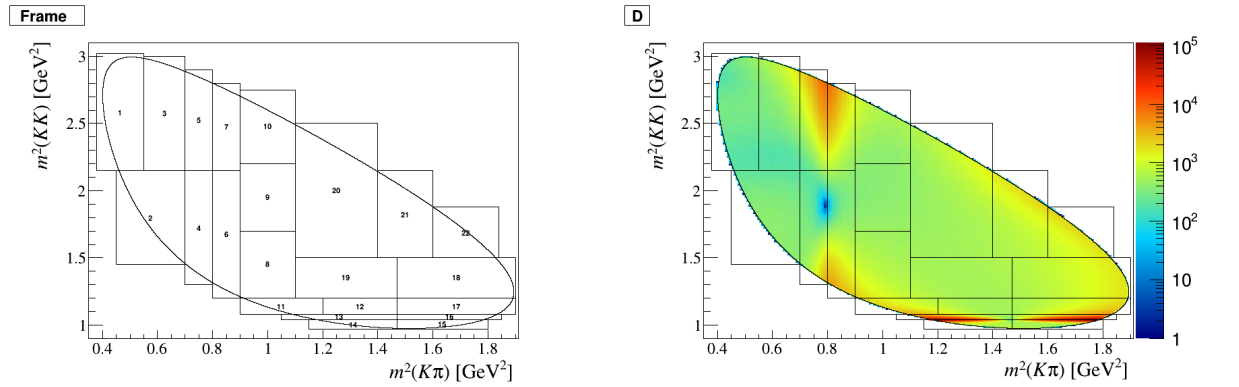

Figure **5-12**.: Left: Scheme showing the binning structure proposed for the physics motivated binning. Right: Physics motivated binning with the DP of a generated ToyMC sample showing the distribution of events across the phase space.

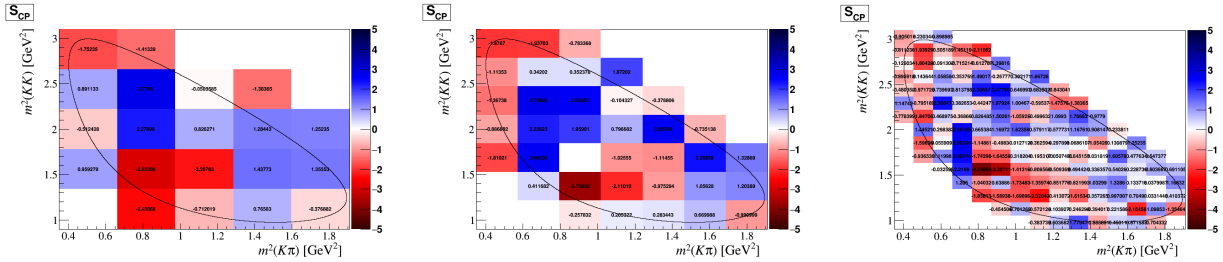

Figure **5-13**.: S_{CP} values on the DP for different number of bins on an uniform binning grid.

5.5. Miranda procedure on the no-asymmetry case

To introduce the sensitivity studies on the full Monte Carlo samples (2×10^8 events for (D^+, D^-)) samples, we start by looking at the null case. That is the case where no asymmetry is introduced on the parameters of the amplitude for each charge. Here the study is done on the three proposed binning schemes with a fixed number of bins; 7×7 bins on the Uniform case, 22 bins on the Adaptive binning and the Physics motivated binning of 22 bins proposed in the previous section. As expected in every case the $p - values$ obtained are between 0.1 and 1 meaning that no significant asymmetry is found between the two samples. it can be seen from figure **5-17** that in every case the distribution of S_{CP} values is approximately centered at 0 and has standard deviation near 1.

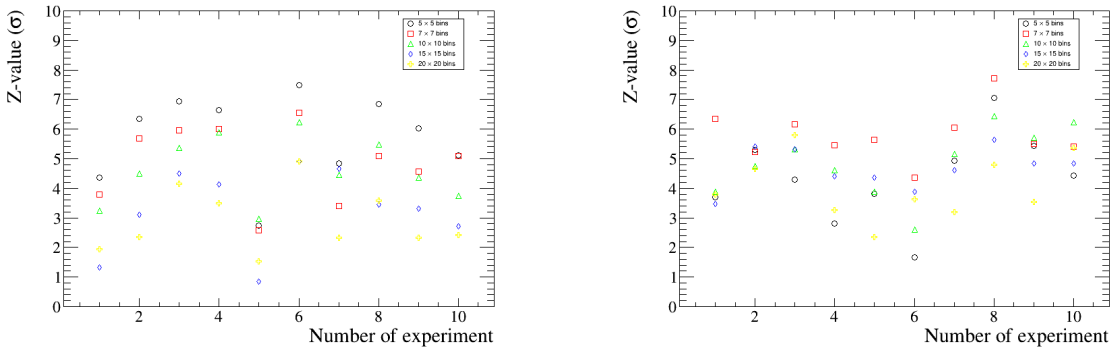

Figure **5-14**.: Z-value obtained for the different samples of asymmetry of $\Delta a = 0.15\%$(left) and of $\Delta\delta = 0.2°$(right) on the K^* for different numbers of bins on the uniform binning.

nbins	15	20	22	25	30
$\Delta a = 0.15°$	6/10	6/10	5/10	6/10	5/10
$\Delta\delta = 0.2°$	1/10	1/10	3/10	2/10	2/10

Table **5-4**.: Number of samples with observed CPV with a significance of 5σ for samples of introduced asymmetry of $\Delta a = 0.15\%$ and of $\Delta\delta = 0.2°$ on the K^*.

5.6. Miranda studies with different levels of asymmetry

Ten samples of 2×10^8 events for (D^+, D^-) are generated introducing a relative difference on the amplitudes and phases of the $K^*(892)$ and $\phi(1020)$. For each of the samples the p-value is calculated and for the cases where $p < 3 \times 10^{-7}$ is considered an observation of CPV at 5σ significance. Results for the Miranda procedure performed using the three binning schemes are summarized as the number of samples where CPV is observed at 5σ significance out of the total 10 samples, in tables **5-5** and **5-6**.

It is observed how the different binning schemes are less sensitive to asymmetries coming from the relative phase, particularly on the $\phi(1020)$ contribution, this can be attributed to the very narrow form of the $\phi(1020)$ lineshape, which makes its phase change very rapidly and makes it harder for the method to identify asymmetries coming from that region. Overall the physical binning method seems to be more sensitive to observation of CPV signals and performing very well on most levels of asymmetry tested. Graphs of S_{CP} distributions for several samples can be found in appendix A. The Z-values obtained for different levels of asymmetry are shown in figures **5-18** and **5-19**.

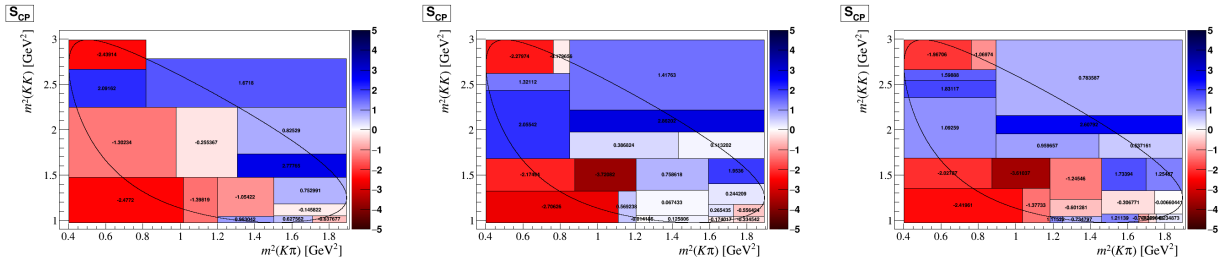

Figure **5-15**.: S_{CP} values on the DP for different number of bins on the adaptive binning scheme.

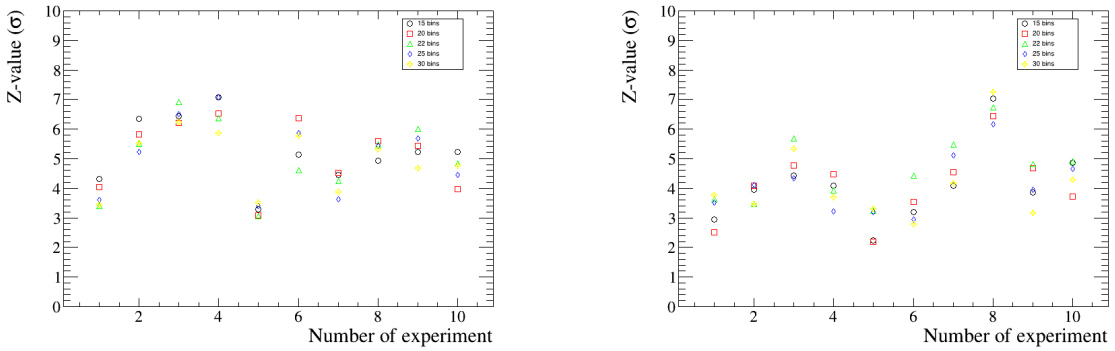

Figure **5-16**.: Z-value obtained for the different samples of asymmetry of $\Delta a = 0.15\%$(left) and of $\Delta\delta = 0.2°$(right) on the K^* for different numbers of bins on the adaptive binning.

5.7. Background

So far, the sensitivity study presented here has only included a signal data set modeled as resonant contributions to the amplitude. Based on previous analysis for this decay channel [44] we expect to have a small, yet significant background contribution over the mass window defined by data selection. Hence, a verification on the purity level that we require for the Miranda study to be sensitive to CPV observation is necessary. A non-resonant background contribution is introduced into our model that is uniform across the Dalitz plot, that is a constant term in the amplitude model.

The purity of a sample is a measure of the amount of total signal that is present, is defined as $S/(S+B)$, being S and B the number of signal and background events respectively. Invariant mass projections of the amplitude model with a purity level of 80% are shown in figure **5-20**. The effect of different amounts of background in the data sample is studied under the Miranda procedure with the different levels of asymmetry as shown before, results

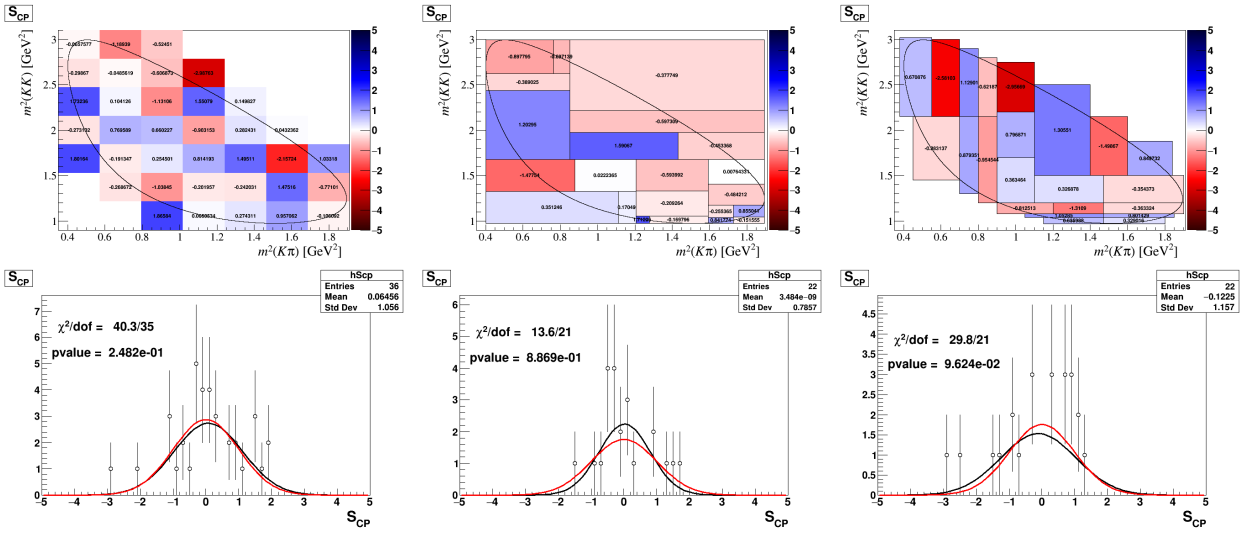

Figure **5-17**.: S_{CP} Dalitz plot on a 7×7 uniform binning grid (left), a 22 bins adaptive binning scheme (center) and a 22 bins physical binning scheme. The distribution of S_{CP} values is shown below. Black line is the Gaussian fitted to the values obtained. Red line is a reference Gaussian with $\mu = 0$ and $\sigma = 1$.

are presented in tables **5-7** and **5-8**.

By looking at the significance distribution we are able to compare how the CPV detection varies slightly by the inclusion of a constant background component. Reducing the $Z-value$ below the 5σ confidence level in some cases. For the cases studied here the physical binning scheme is the one that is best able to distinguish these effects from the S_{CP} distribution across the Dalitz plot. Results for the significance obtained for the Physical binning scheme are shown in figure **5-21**.

In Chapter 5 a study of the asymmetry on the sidebands for the real decays $D_(s)^+ \to K^-K^+\pi^+$ with the objective of verifying that no observable asymmetry comes from this region of the mass window. As a further study on the sensitivity we also perform an analysis of the Miranda procedure using a weighted sample of the combined sidebands for the $D^+ \to K^-K^+\pi^+$ mode using a purity level of $\sim 10\%$. Results are shown in table **5-9** and **5-10**, Z-value distributions compared with the no background case are shown in figure **5-22**.

$K^*(892)$			
$\Delta a(\%)$	Uniform	Adaptive	Physical
0.1	0/10	1/10	0/10
0.15	6/10	5/10	8/10
0.2	10/10	10/10	10/10
0.3	10/10	10/10	10/10

$K^*(892)$			
$\Delta\delta(^\circ)$	Uniform	Adaptive	Physical
0.1	0/10	0/10	0/10
0.15	3/10	0/10	3/10
0.2	9/10	3/10	9/10
0.3	10/10	10/10	10/10

Table **5-5**.: Results on the number of samples with observed CPV at 5σ significance out of a total of 10 samples for the three binning schemes on different levels of asymmetry introduced on the amplitude (left) and phase (right) of the $K^*(892)$ resonance.

$\phi(1020)$			
$\Delta a(\%)$	Uniform	Adaptive	Physical
0.1	0/10	0/10	0/10
0.15	0/10	6/10	5/10
0.2	9/10	10/10	10/10
0.3	10/10	10/10	10/10

$\phi(1020)$			
$\Delta\delta(^\circ)$	Uniform	Adaptive	Physical
0.1	0/10	0/10	0/10
0.2	0/10	2/10	5/10
0.3	3/10	7/10	9/10
0.4	8/10	10/10	10/10

Table **5-6**.: Results on the number of samples with observed CPV at 5σ significance out of a total of 10 samples for the three binning schemes on different levels of asymmetry introduced on the amplitude (left) and phase (right) of the $\phi(1020)$ resonance.

5.8. Data selection

Selection criteria applied to the LHCb Run II data set must be the same for the D^+ and D_s^+ decays. Cuts applied to data must be choosen so that it maximizes the elimination of background contributions from other channels and miss-identified particles while ensuring minimal loss of the signal. For this analysis a mass window of $1805 \leq M_D < 1935$ for the D_s^+ and a mass window of $1905 \leq M_D < 2035$ for the control channel, the D_s^+ is used. From particle identification of the final states is required that the probability of classifying the kaons and pions as such to be greater than 0.3 for the three final states, defined by the variables $p(1,2)\_ProbNNk > 0.3$ and $p3\_ProbNNpi > 0.3$. Identification should also avoid the inclusion of D^+ mesons that come from decays $B \to DX$ since it would introduce asymmetries coming from B decays. This is achieved by computing the displacement of the track of the mother particle from the primary vertex, the impact parameter (IP), and form a χ^2 under the hypothesis that IP is 0, the cut $\chi^2_{(IP)} < 8$ is applied.

To reduce specific background contributions, vetos on certain decay modes must be applied. A veto on the identification of the third particle as a muon is also done to restrict semi-

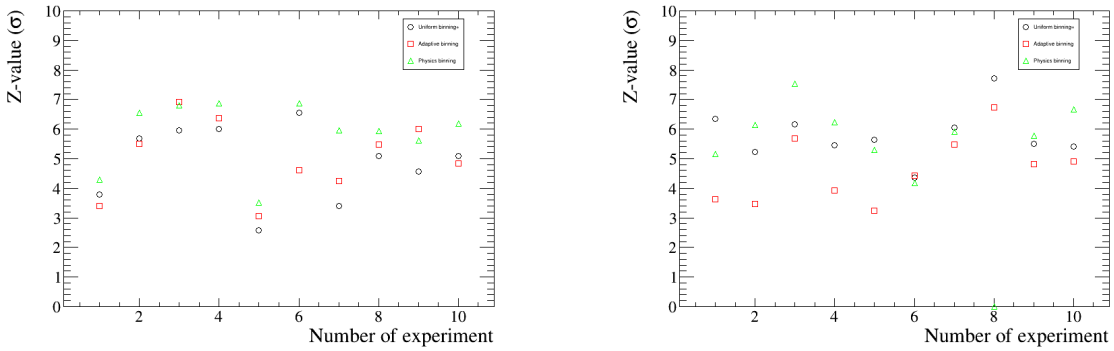

Figure **5-18**.: Statistical significance for the different experiments produced with asymmetry of $\Delta a = 0.15\%$(left) and $\Delta\delta = 0.2°$(right) along the K^*.

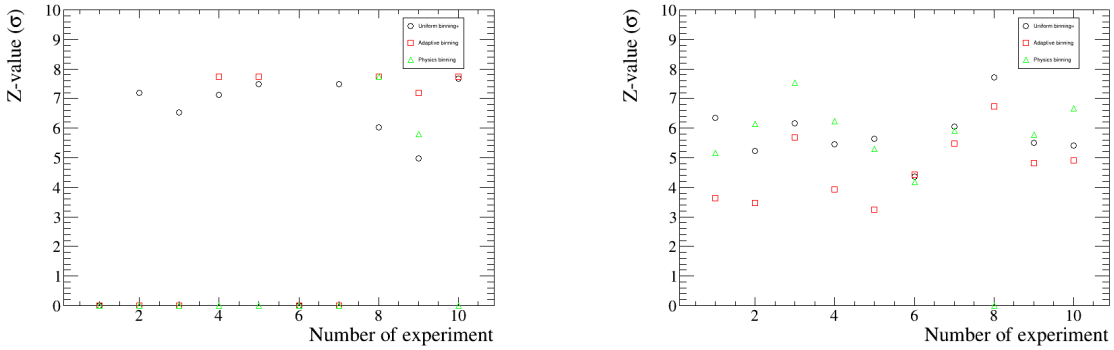

Figure **5-19**.: Statistical significance for the different experiments produced with asymmetry of $\Delta a = 0.2\%$(left) and $\Delta\delta = 0.3°$(right) along the ϕ.

leptonic decay contributions. Other contamination contributions that are subtracted are the miss-identification of the K^+ as a proton p in the decay $\Lambda_c^+ \to K^-p\pi^+$ by performing a cut on the wrong mass identification $|m_{Kp\pi} - 2288MeV/c^2| > 13MeV/c^2$, the wrong identification of one of the kaons as a pion is done by tightening the particle identification of the first to particles as a kaon $(p_1, p_2)\_PIDK > 15$, contributions coming from $D^0 \to K^-K^+$ decays are also cut by imposing the condition on the invariant mass of the K^-K^+ system $m_{K^-K^+} < 1.85GeV/c^2$.

Finally, to control production asymmetries on the Dalitz plot fiducial cuts on the kinematic variables of the final state particles are performed. Cuts on the momentum components of

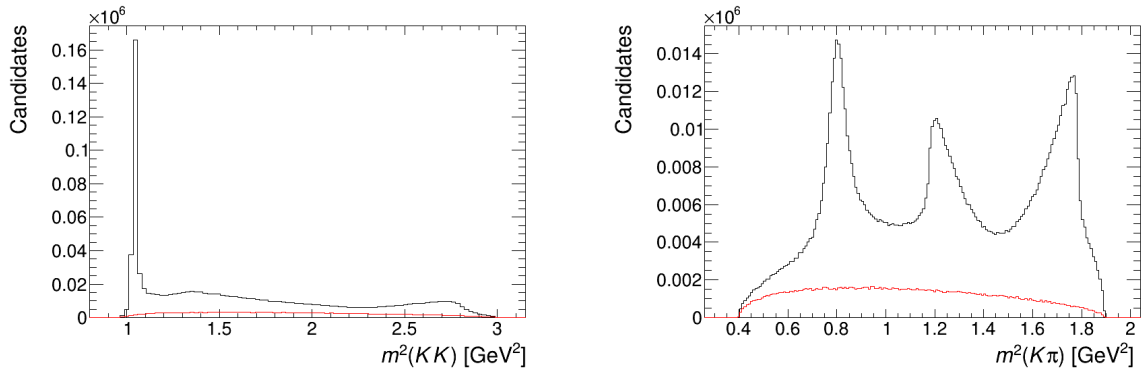

Figure **5-20**.: Invariant mass projections of a sample generated with a purity level of 0.8. Background component is show in red.

$\Delta a = 0.15\%(K^*(892))$			
Purity (%)	Uniform	Adaptive	Physical
80	6/10	3/10	8/10
90	5/10	4/10	8/10
95	5/10	7/10	8/10
100	6/10	7/10	8/10

$\Delta\delta = 0.2°(K^*(892))$			
Purity (%)	Uniform	Adaptive	Physical
80	6/10	1/10	4/10
90	4/10	2/10	7/10
95	9/10	3/10	9/10
100	9/10	3/10	9/10

Table **5-7**.: Results on the number of samples with observed CPV at 5σ significance out of a total of 10 samples for the three binning schemes on different levels of asymmetry introduced on the amplitude (left) and phase (right) of the $K^*(892)$ resonance for different level of purity using a constant non-resonant term.

the final states are performed as

$$p_{(1,2)z} > 3.57 \times \left|p_{(1,2)x}\right| + 1000MeV/c, \tag{5-3}$$
$$p_{3z} > 3.07 \times (|p_{3x}| - 500MeV/c) + 3000Mev/c, \tag{5-4}$$
$$p_{(1,2)z} > 4.25 \times \left|p_{(1,2)y}\right|, \tag{5-5}$$
$$p_{3z} > 4.0 \times |p_{3y}|, \tag{5-6}$$
$$p_{(1,2)z} > 4000MeV/c. \tag{5-7}$$

5.9. Asymmetry on the sidebands

In the Miranda studies that will be performed on the decay channel $D^+ \to K^-K^+\pi^+$ is important to verify that any possible asymmetry signal that may appear will come only

$\Delta a = 0.15\%(\phi(1020))$				$\Delta\delta = 0.3^\circ(\phi(1020))$			
Purity (%)	Uniform	Adaptive	Physical	Purity (%)	Uniform	Adaptive	Physical
80	1/10	2/10	4/10	80	0/10	8/10	8/10
90	0/10	4/10	4/10	90	2/10	7/10	9/10
95	0/10	4/10	5/10	95	3/10	8/10	10/10
100	0/10	6/10	5/10	100	3/10	7/10	10/10

Table **5-8**.: Results on the number of samples with observed CPV at 5σ significance out of a total of 10 samples for the three binning schemes on different levels of asymmetry introduced on the amplitude (left) and phase (right) of the $\phi(1020)$ resonance for different level of purity using a constant non-resonant term.

$\Delta a = 0.15\%(K^*(892))$				$\Delta\delta = 0.2^\circ(K^*(892))$			
Purity (%)	Uniform	Adaptive	Physical	Purity (%)	Uniform	Adaptive	Physical
90	5/10	7/10	8/10	90	7/10	3/10	7/10
100	6/10	7/10	8/10	100	9/10	3/10	9/10

Table **5-9**.: Results on the number of samples with observed CPV at 5σ significance out of a total of 10 samples for the three binning schemes on different levels of asymmetry introduced on the amplitude (left) and phase (right) of the $K^*(892)$ resonance for different level of purity using weighted events from the sidebands on real data.

from the signal region and not from the background contributions. The crosscheck on these regions is performed by analyzing the behavior of the lower and upper sidebands for each of the decay channels, both control and signal modes, under the Miranda procedure.

For this analysis, a definition of the sidebands is needed such that there is as little interference from the signal lineshape as possible. The mass windows defined for each decay mode of the $K^-K^+\pi^+$ final state is shown in figure **5-23** . The D^+ lower sideband is defined as $1810 < D_M < 1830$ the upper D^+ and lower D_s^+ sidebands are defined using $1910 < D_M < 1930$ and the upper D_s^+ sideband is defined as $2010 < D_M < 2030$. Dalitz plot for each of these regions are shown in figure **5-24**.

The study is done under three different binning schemes, an uniform binning, an adaptive binning where each of the bins have the same number of events, and a physics motivated binning as shown in the previous chapter. Analysis on the S_{CP} significance is performed, results are shown in table **5-11** for the D^+ mode and on table **5-12** for the D_s^+ mode.

In the analysis performed of the Miranda procedure for the three different binning schemes

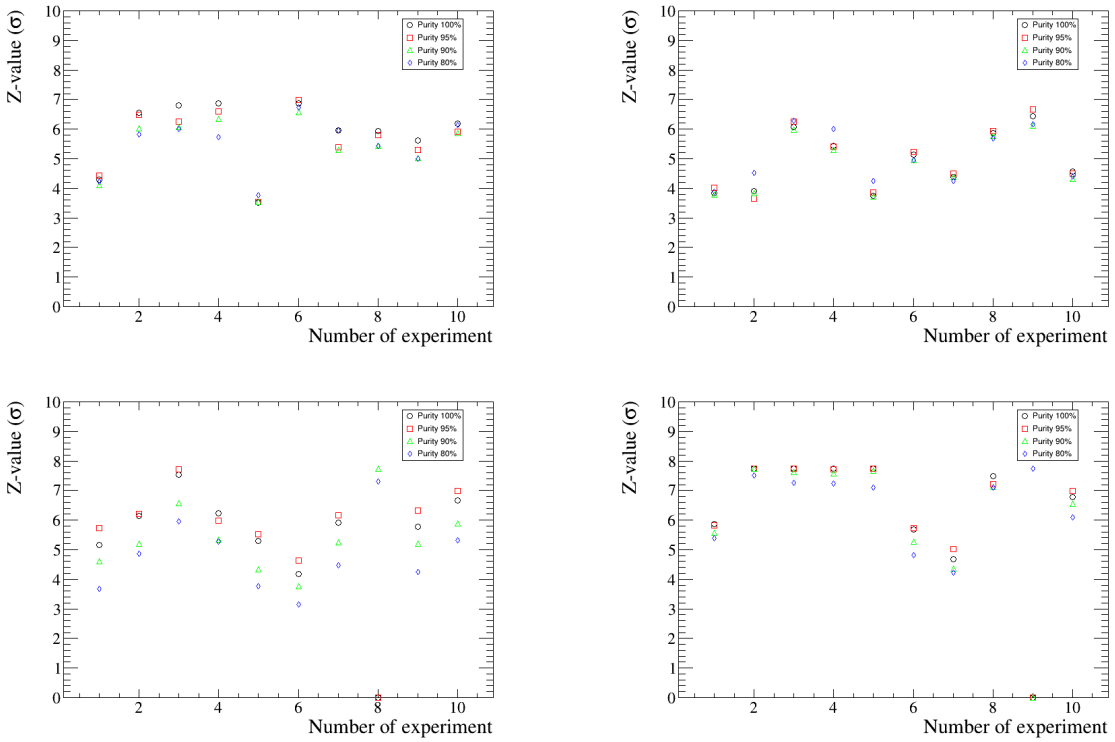

Figure **5-21**.: Z-values distribution for the 10 samples studied under different purity levels for the introduced asymmetries $\Delta a = 0.15\%$ on $K^*(892)$ (top left), $\Delta a = 0.15\%$ on $\phi(1020)$ (top right), $\Delta\delta = 0.2°$ on $K^*(892)$ (bottom left) and $\Delta\delta = 0.3°$ on $\phi(1020)$ (bottom right).

a significant asymmetry is not observed, indicating that any asymmetries found on the data samples used would come mainly from CPV effect or production asymmetries on the signal region and not from the background. Next steps on the Miranda analysis would be to study the asymmetries on the signal region of the control channel to verify that no production asymmetries may come from the $K^-K^+\pi^+$ signal region. In case such a production asymmetry is found, a method for factorizing the production asymmetries would be needed in order to observe physical CPV effects on the D^+ decay mode.

$\Delta a = 0.15\%(\phi(1020))$			
Purity (%)	Uniform	Adaptive	Physical
90	0/10	7/10	7/10
100	0/10	6/10	5/10

$\Delta\delta = 0.3^\circ(\phi(1020))$			
Purity (%)	Uniform	Adaptive	Physical
90	2/10	7/10	9/10
100	3/10	7/10	10/10

Table **5-10**.: Results on the number of samples with observed CPV at 5σ significance out of a total of 10 samples for the three binning schemes on different levels of asymmetry introduced on the amplitude (left) and phase (right) of the $\phi(1020)$ resonance for different level of purity using weighted events from the sidebands on real data.

	Uniform binning		Adaptive binning		Physical binning	
	$\chi^2/ndof$	p-value(%)	$\chi^2/ndof$	p-value(%)	$\chi^2/ndof$	p-value(%)
Lower sideband	28.37/35	77.86	15.74/21	78.40	21.73/21	41.50
Upper sideband	44.0/35	14.16	38.99/21	0.99	34.10/21	3.53
Combined sidebands	36.93/35	37.99	47.34/21	0.08	35.20/21	2.68

Table **5-11**.: Results of the Miranda procedure applied on three different binning schemes, uniform, adaptive and pyshical. For the $D^+ \to K^-K^+\pi^+$ decay mode.

	Uniform binning		Adaptive binning		Physical binning	
	$\chi^2/ndof$	p-value(%)	$\chi^2/ndof$	p-value(%)	$\chi^2/ndof$	p-value(%)
Lower sideband	40.52/34	20.47	35.99/21	2.19	34.24/21	3.41
Upper sideband	56.20/34	0.97	57.67/21	2.86×10^{-3}	45.0/21	0.17
Combined sidebands	54.56/34	1.41	69.73/21	3.88×10^{-5}	42.01/21	0.42

Table **5-12**.: Results of the Miranda procedure applied on three different binning schemes, uniform, adaptive and pyshical. For the $D_s^+ \to K^-K^+\pi^+$ decay mode.

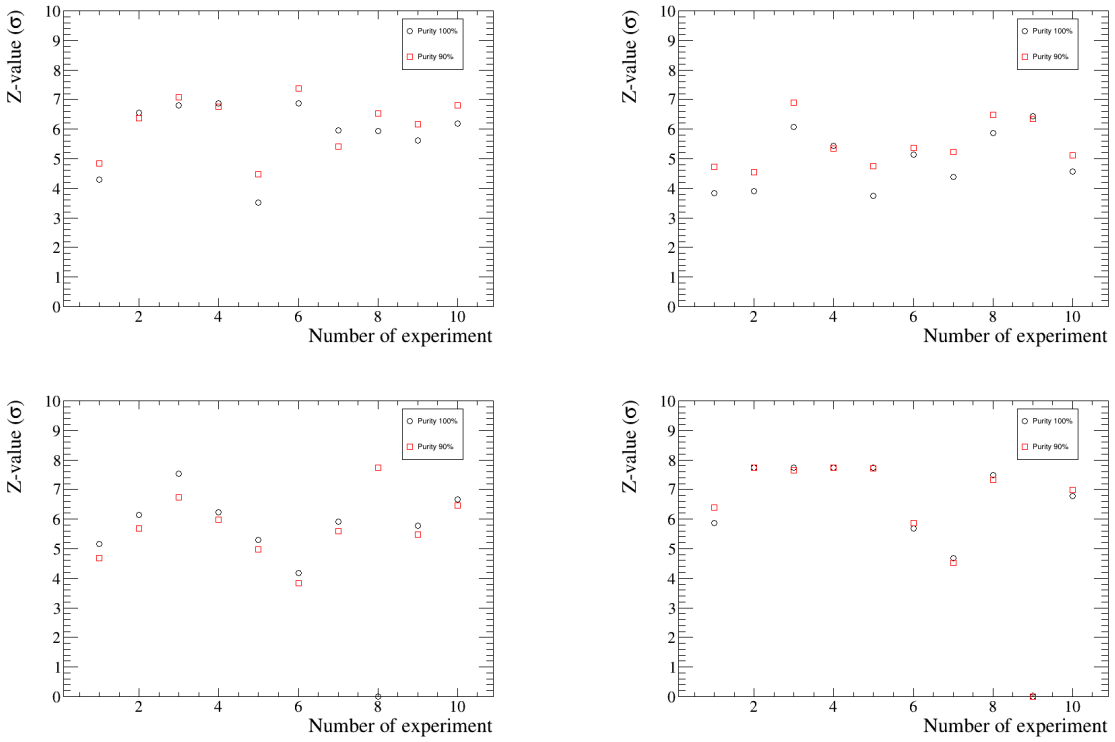

Figure **5-22**.: Z-values distribution for the 10 samples studied under different purity levels for the introduced asymmetries $\Delta a = 0.15\%$ on $K^*(892)$ (top left), $\Delta a = 0.15\%$ on $\phi(1020)$ (top right), $\Delta\delta = 0.2°$ on $K^*(892)$ (bottom left) and $\Delta\delta = 0.3°$ on $\phi(1020)$ (bottom right) using weighted events from the sidebands of real data.

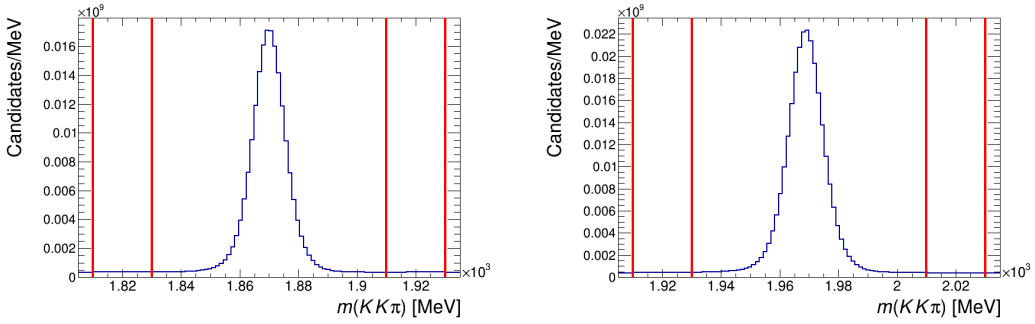

Figure **5-23**.: Mass spectrum of the $D^+ \to K^-K^+\pi^+$ (left) and $D_s^+ \to K^-K^+\pi^+$ (right). The mass windows for each sidebands are bounded by the red vertical lines.

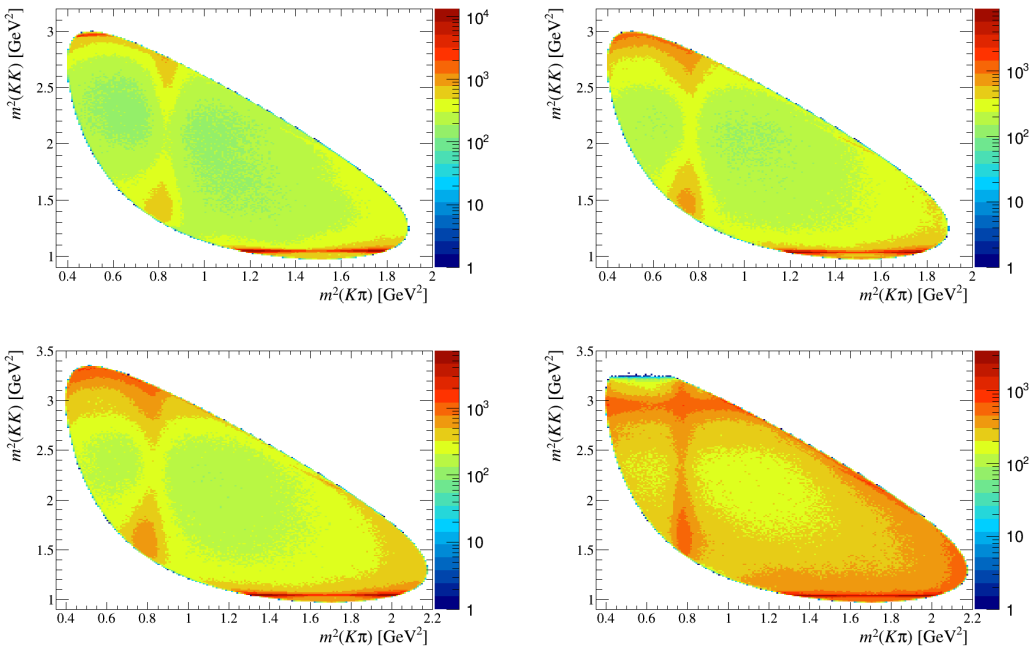

Figure **5-24**.: Dalitz plot for the sidebands regions of the D^+ lower (top left) and upper (top right) sidebands and the D_s^+ lower (bottom left) and upper sidebands (bottom right).

6. Conclusions

The decay channel $D^+ \to K^-K^+\pi^+$ is expected to have a large signal data size on the LHCb Run II with a considerable high purity. Sensitivity studies are a fundamental first step for understanding the levels of asymmetry that may be observed in the data sample and the best binning strategy for the detection of such effects. Using the CLEO model description for the decay channel, toy Monte Carlo samples of 2×10^8 events of (D^+, D^-) were generated and studied using the Miranda procedure. CPV effects can be measured at the 5σ confidence level coming from variations on the relative amplitude of the $K^*(892)$ or $\phi(1020)$ resonance of $\Delta A = 0.2\%$, showing significant CPV effects on every sample. For asymmetries coming from the relative phases a good probability of observation is shown at $\Delta\phi = 0.2^\circ$ for the $K^*(892)$ while for the $\phi(1020)$ a difference of phase $\Delta\phi = 0.4^\circ$ is needed for having a good CPV observation probability. This dependence can be explained as the very narrow shape of the $\phi(1020)$ resonance makes its phase change rapidly so that phase differences will be less significative than on the wider $K^*(892)$. Studies including an uniform background component for samples with a purity level of $\sim 90\%$ show no significant change in the sensitivity of the Miranda procedure given that no considerable asymmetry effects come from the background. Using weighted events from the sidebands of the real LHCb run II data set shows similar results. It is concluded that at the expected purity level of $\sim 90\%$ no significant changes in the sensitivity are expected.

The physics motivated binning scheme appears to be able to observe asymmetries beyond these effects and proves to be the most efficient binning scheme for detecting asymmetries on the DP while also producing good results when a background component is included at the purity level of 90%. Significant variations on the sensitivity to CPV are observed depending on the binning structure used for the Miranda procedure. It is observed that a naive adaptive binning may make the analysis blind to the physical structure coming from the resonances of the decay that can average away the asymmetry effects observed in the S_{CP} distribution.

The application of the Miranda procedure on the sidebands of data samples for the $D^+ \to K^-K^+\pi^+$ and the control mode $D_s^+ \to K^-K^+\pi^+$ show that no CPV effects can be expected from the background of the decay modes. So any asymmetry effects may come only from

physical or production effects on the signal region.

A. Miranda plots

A.1. Sensitivity studies on the signal model

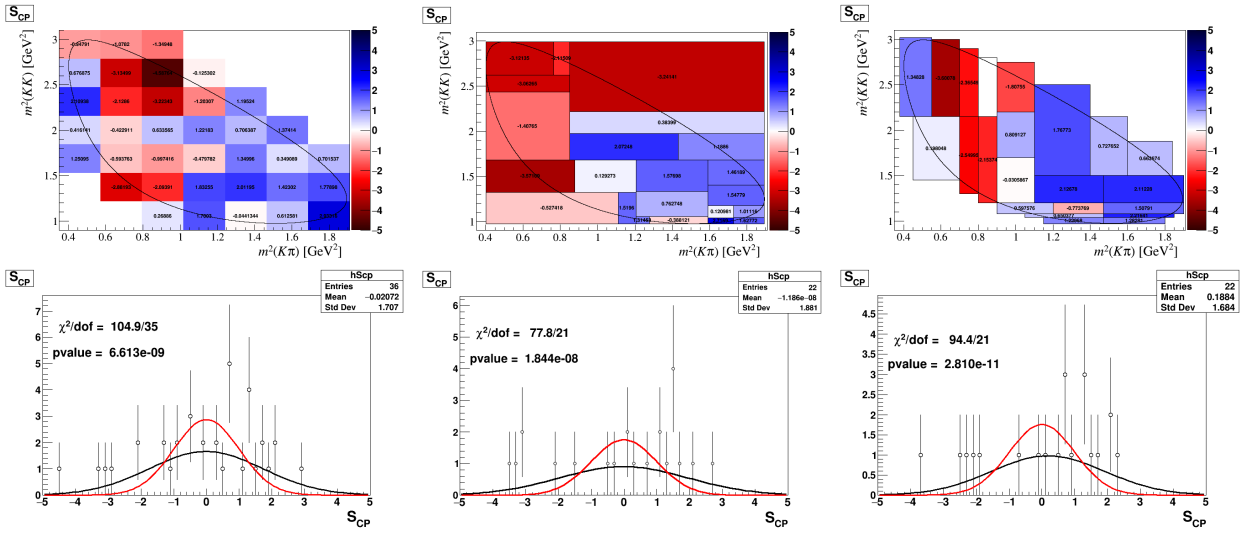

$\Delta a = 0.15\%$ on $K^*(892)$

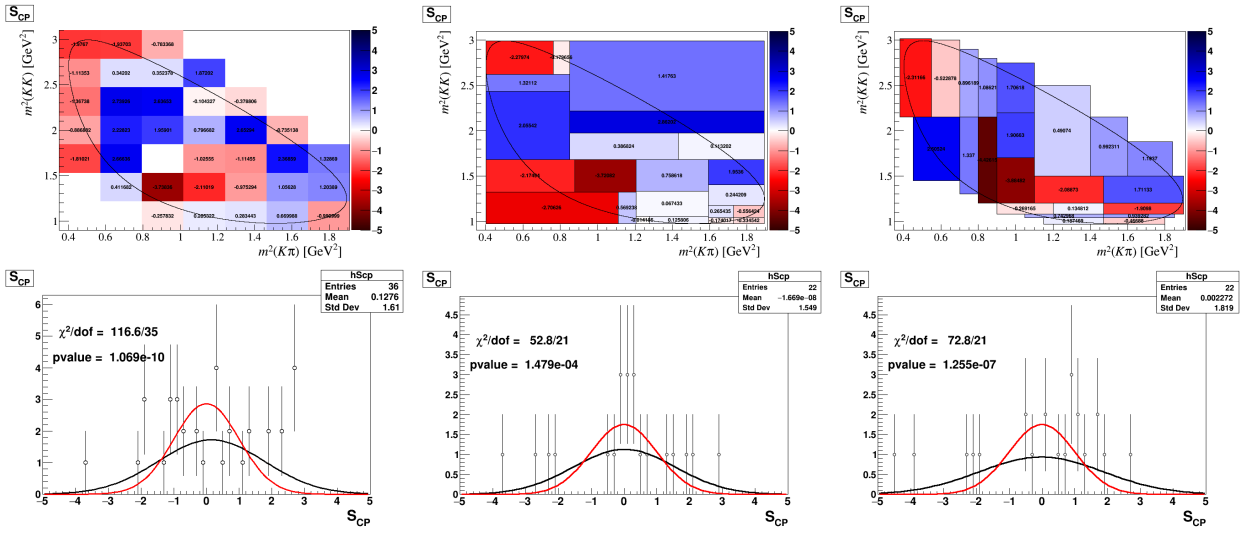

$\Delta\delta = 0.2^\circ$ on $K^*(892)$

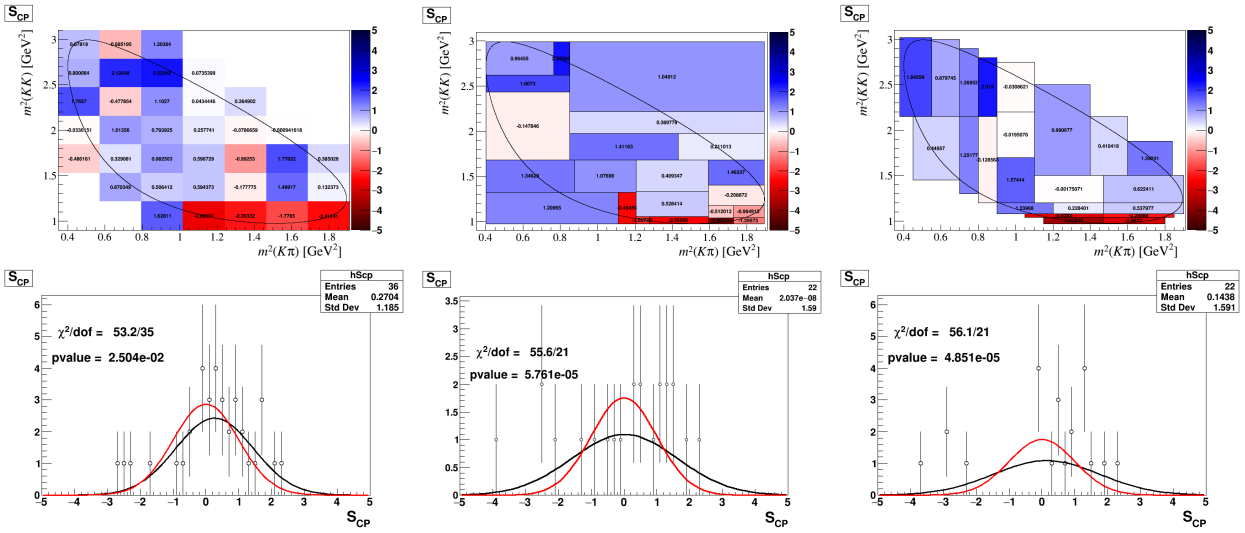

$\Delta a = 0.15\%$ on $\phi(1020)$

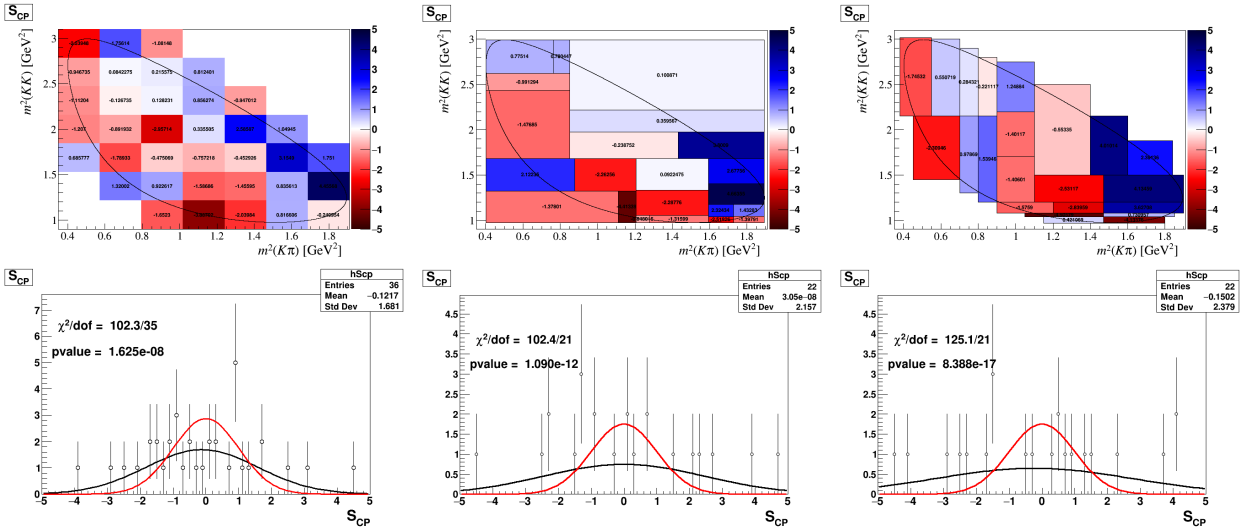

$\Delta\delta = 0.3^\circ$ on $\phi(1020)$

A.2. Sensitivity studies including a background model

A.2.1. Studies with uniform background component

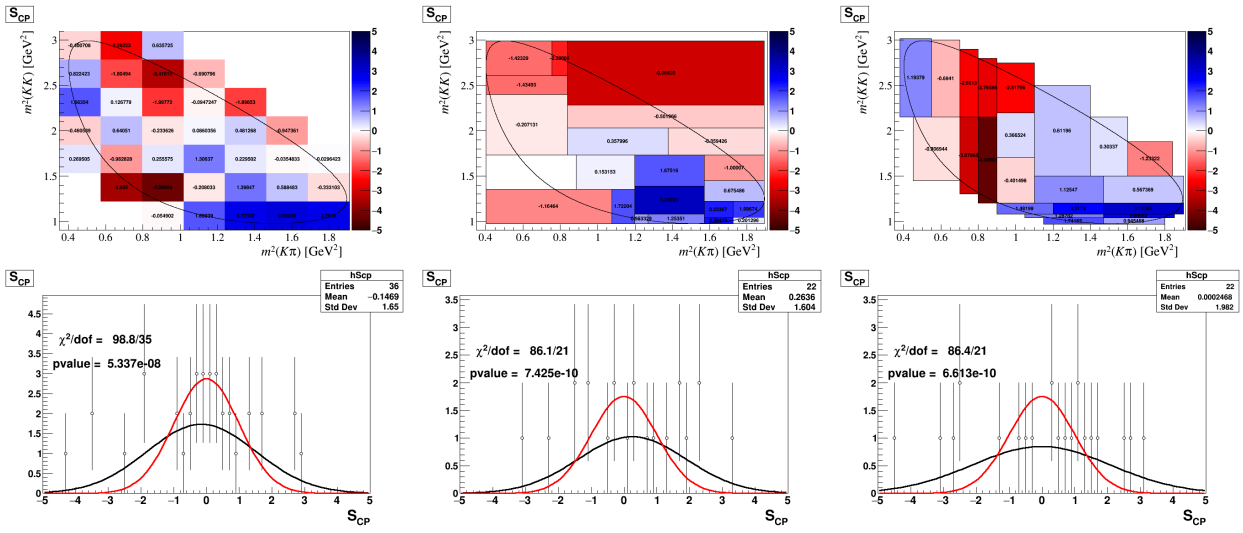

$\Delta a = 0.15\%$ on $K^*(892)$ with an uniform background component, 90% Purity.

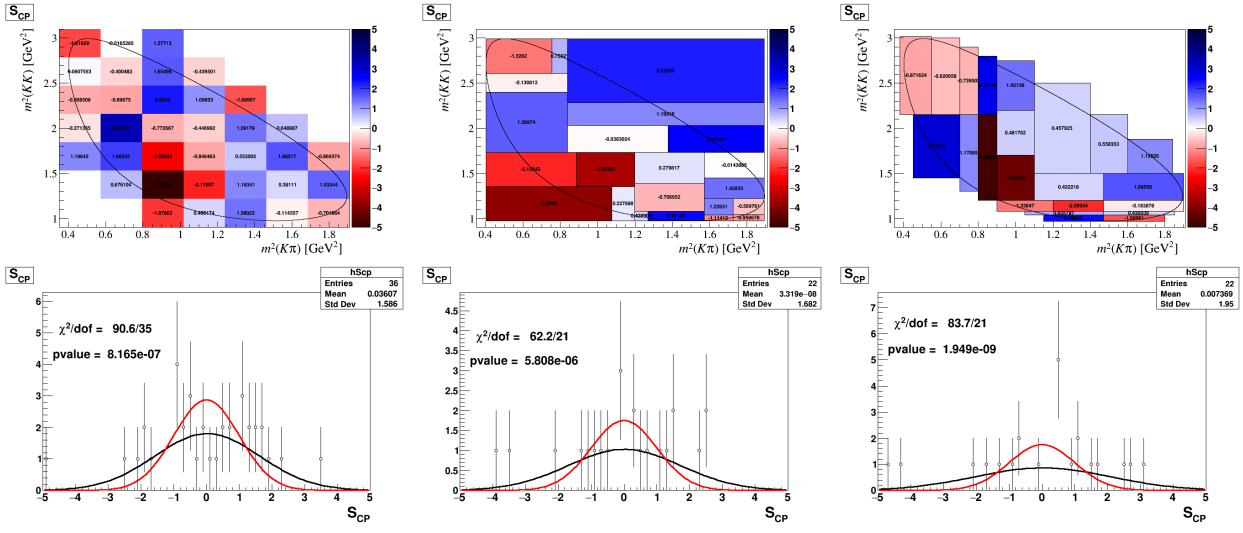

$\Delta\delta = 0.2^\circ$ on $K^*(892)$ with an uniform background component, 90% Purity.

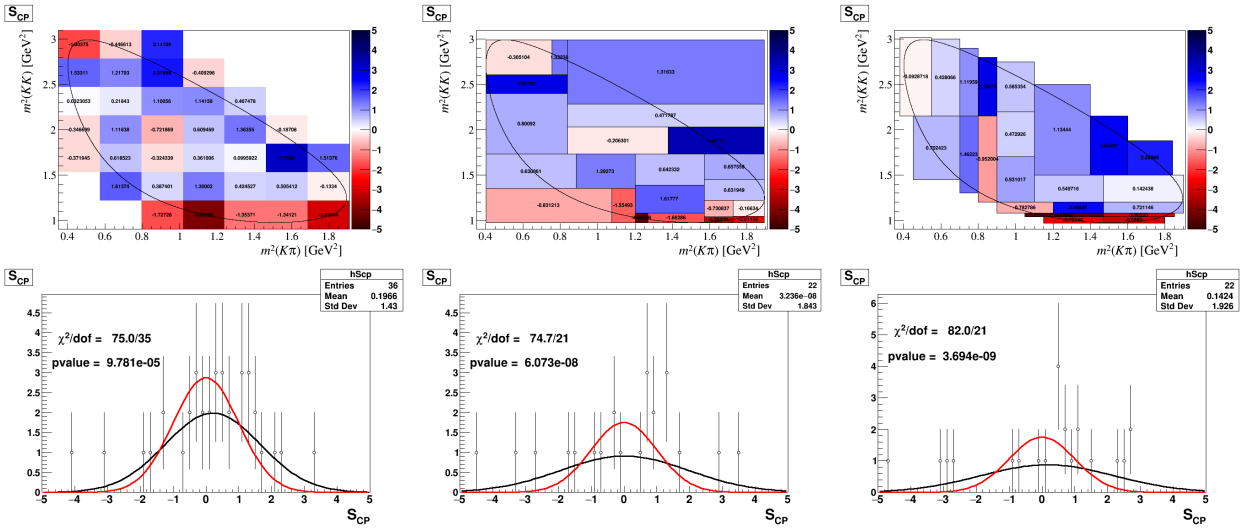

$\Delta a = 0.15\%$ on $\phi(1020)$ with an uniform background component, 90% Purity.

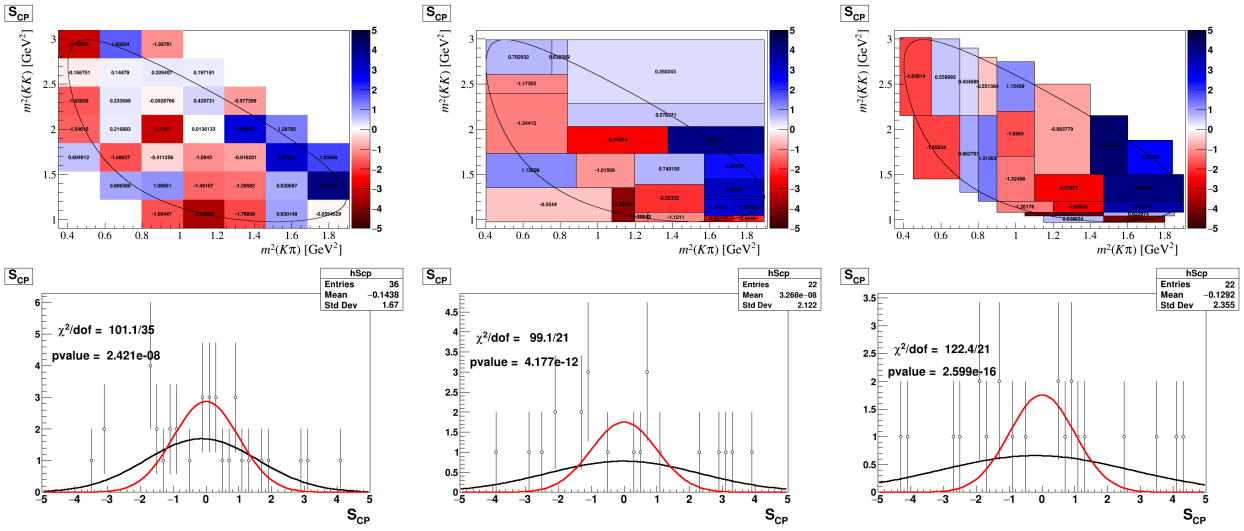

$\Delta\delta = 0.3^\circ$ on $\phi(1020)$ with an uniform background component, 90% Purity.

A.2.2. Studies with data from the sidebands

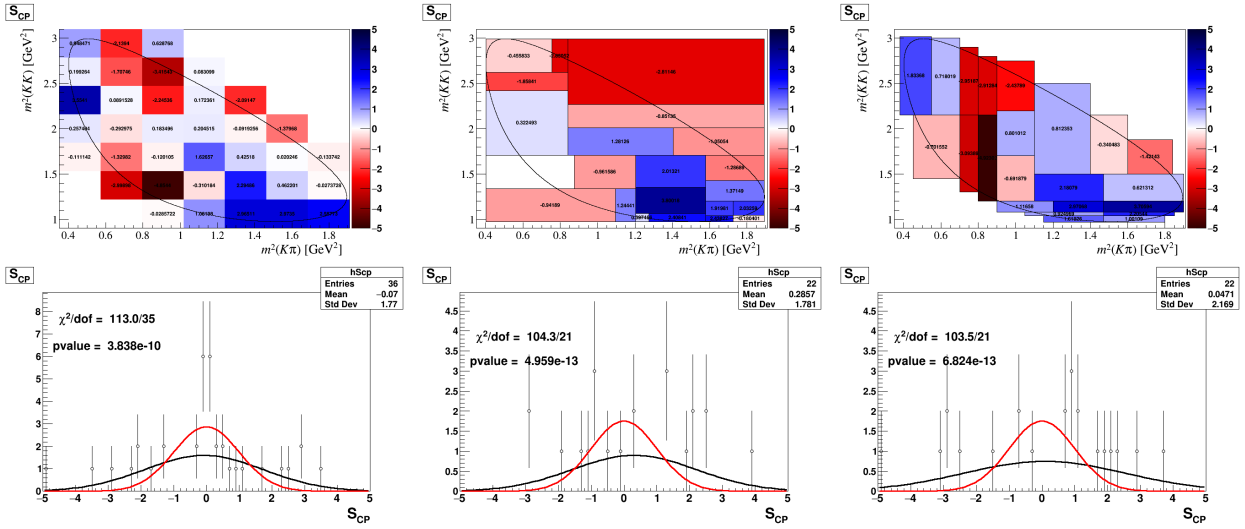

$\Delta a = 0.15\%$ on $K^*(892)$ with weighted sidebands events, 90% Purity.

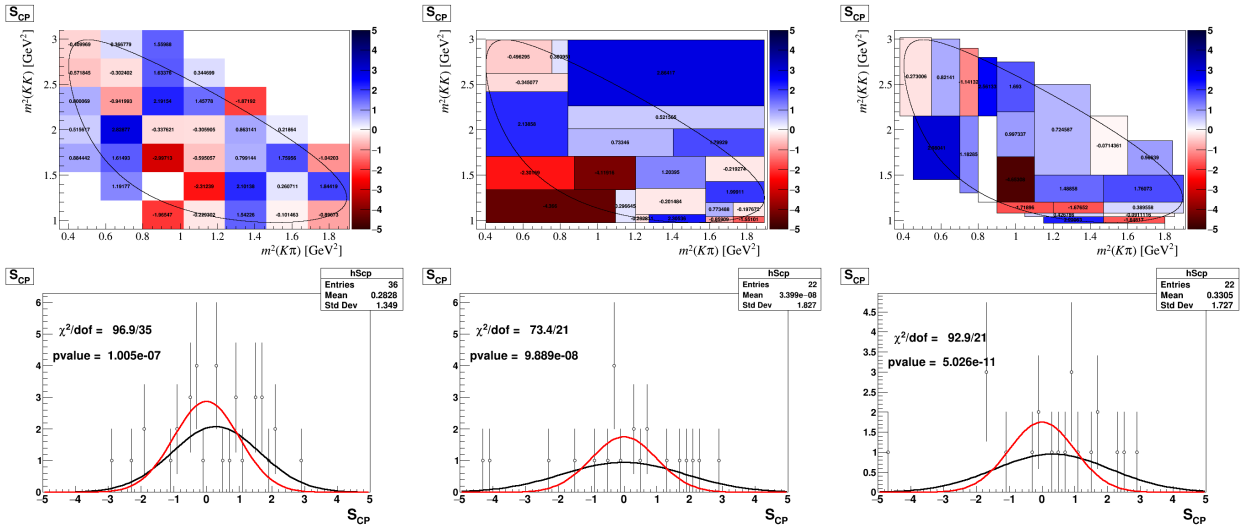

$\Delta\delta = 0.2^\circ$ on $K^*(892)$ with weighted sidebands events, 90% Purity.

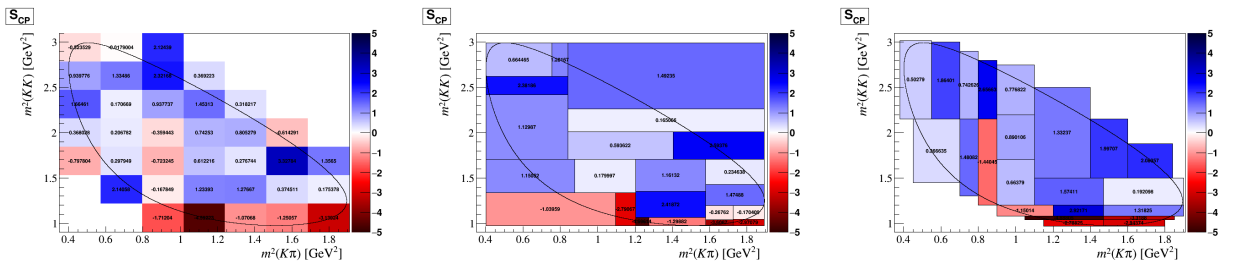

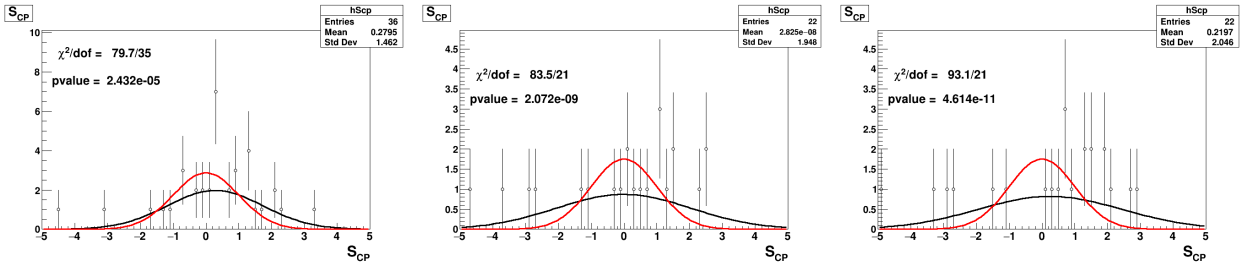

$\Delta a = 0.15\%$ on $\phi(1020)$ with weighted sidebands events, 90% Purity.

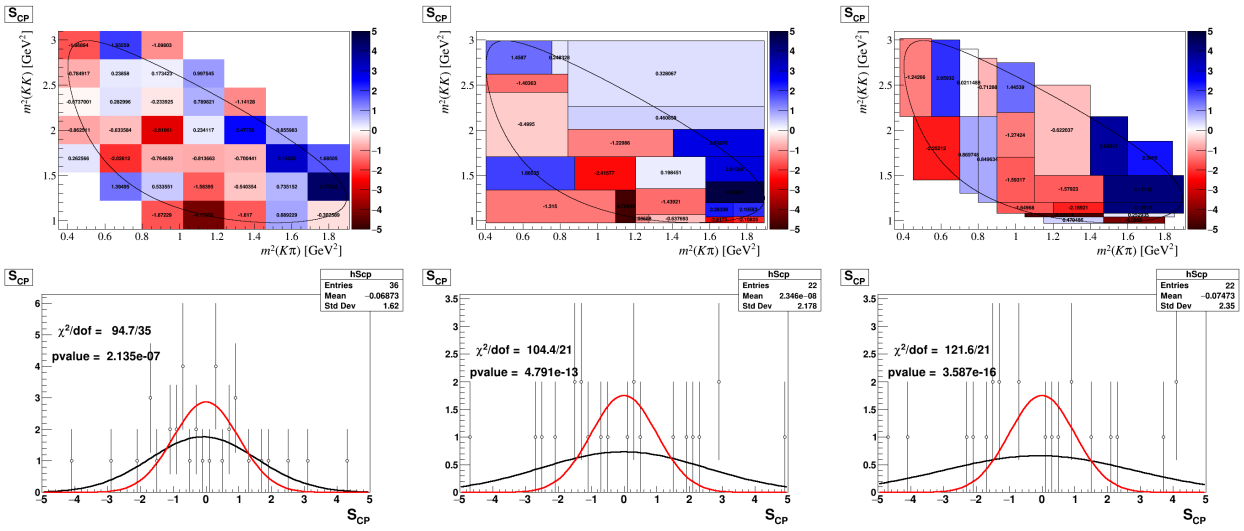

$\Delta\delta = 0.3^\circ$ on $\phi(1020)$ with weighted sidebands events, 90% Purity.

A.3. Miranda analysis on the sidebands

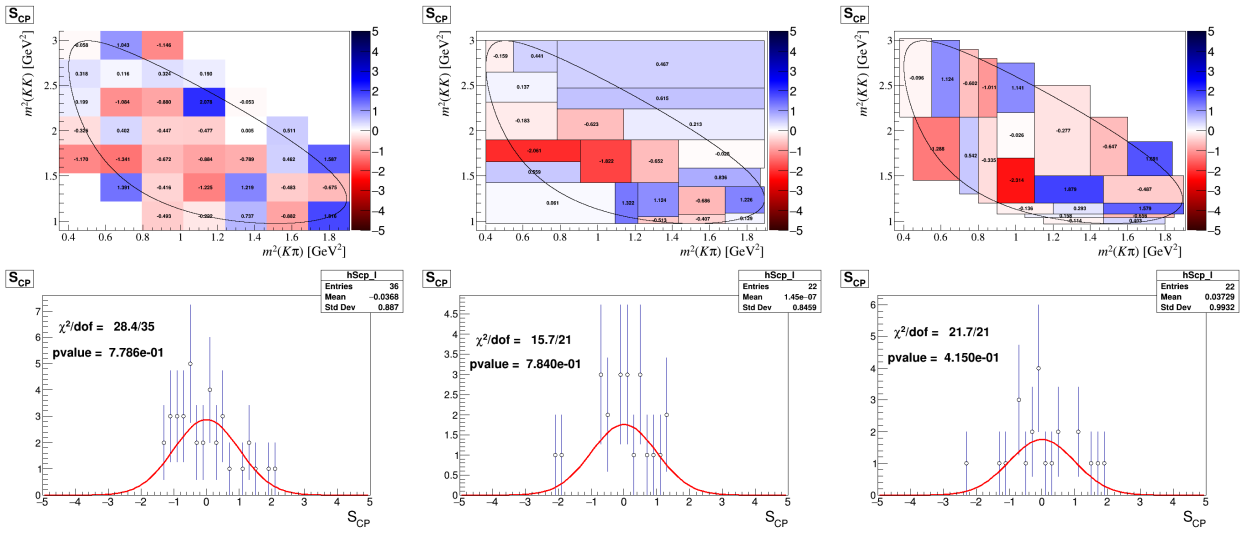

D^+ lower sideband.

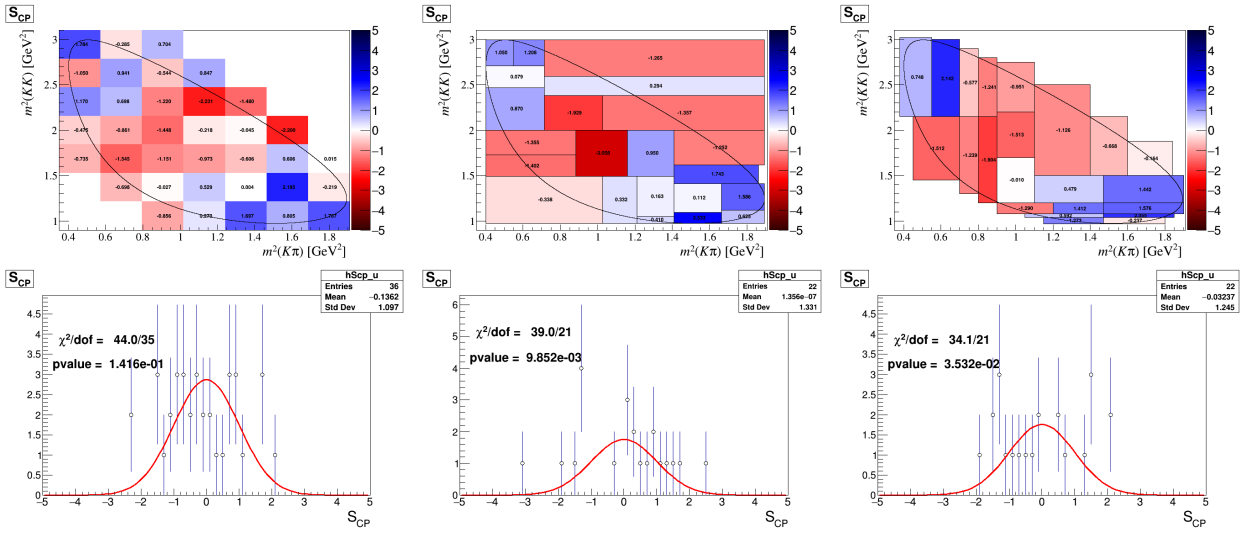

D^+ upper sideband.

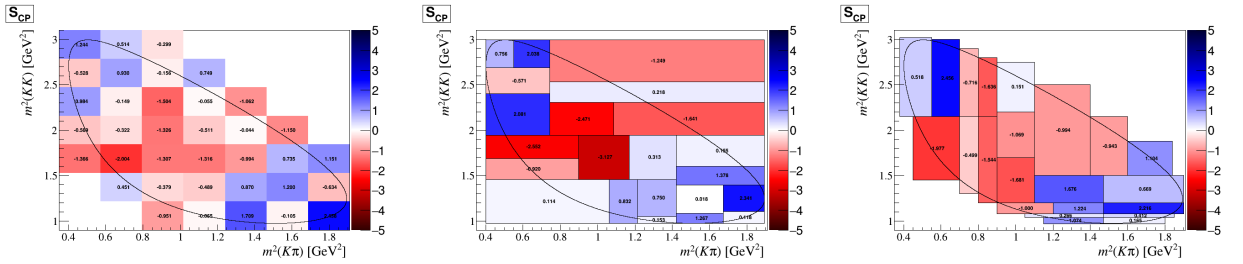

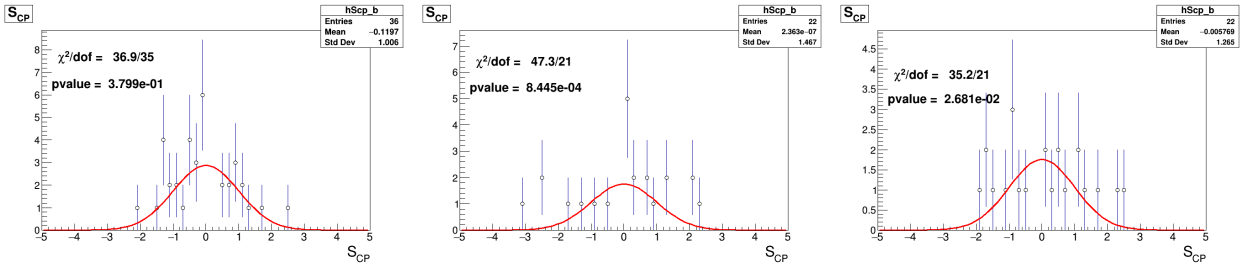

D^+ combined sidebands.

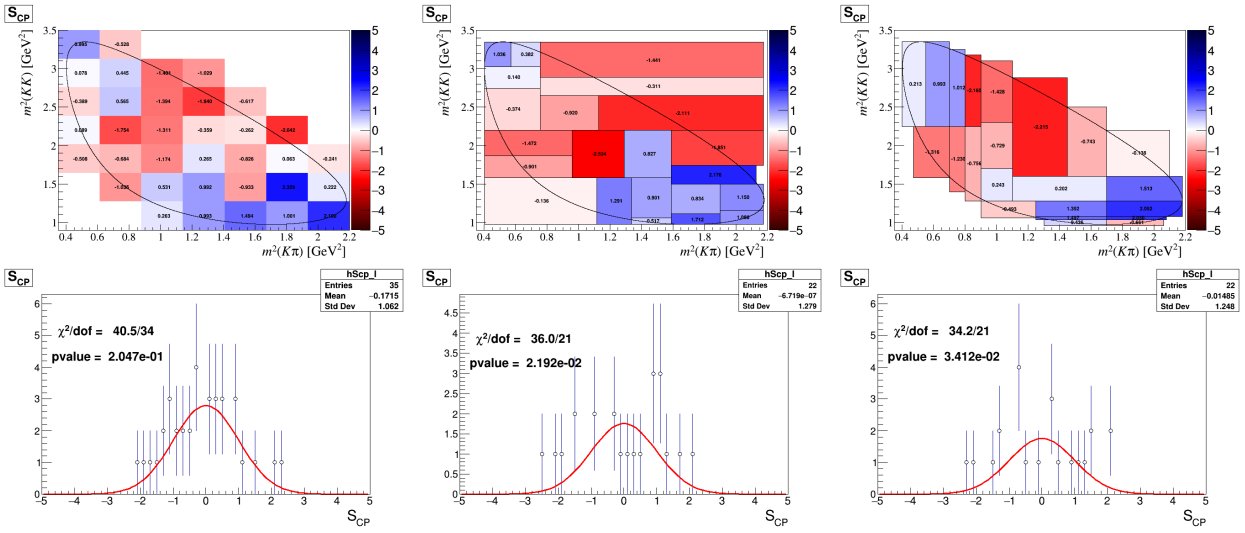

D_s^+ lower sideband.

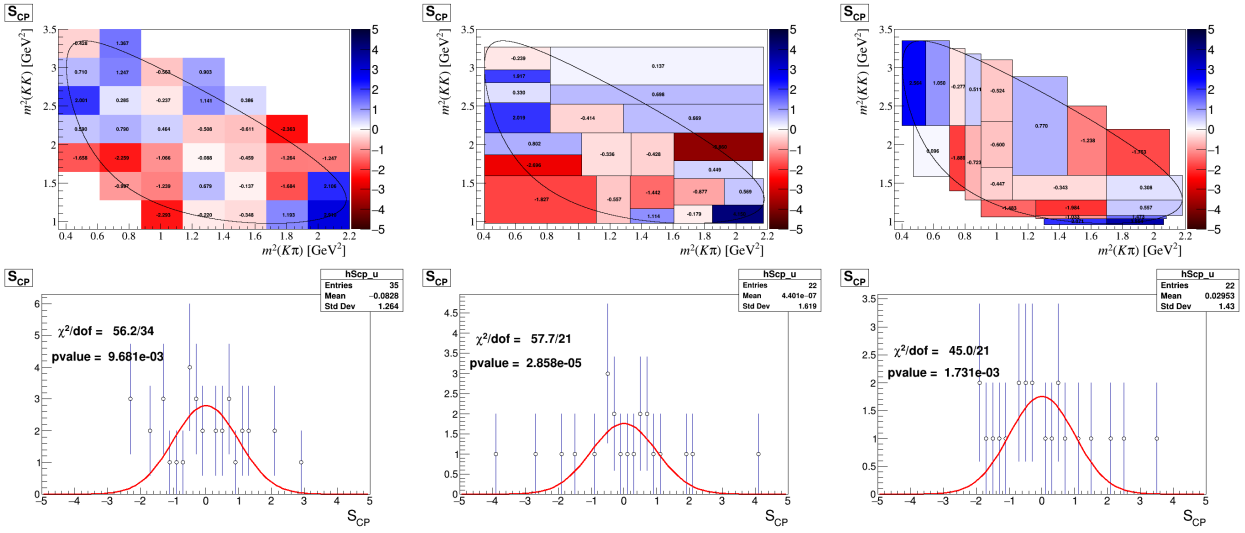

D_s^+ upper sideband.

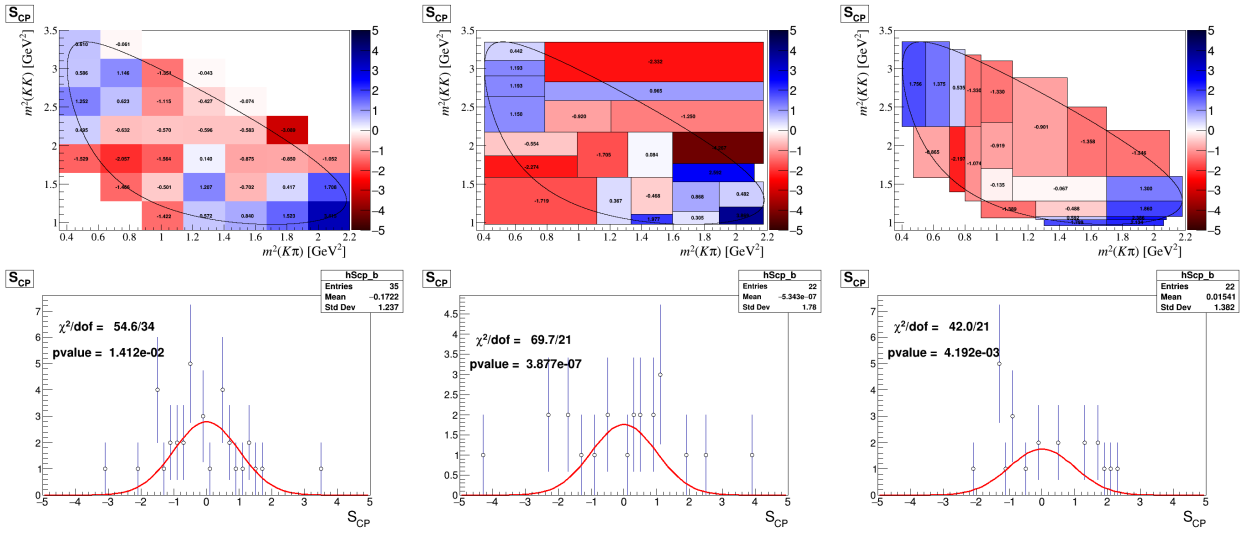

D_s^+ combined sidebands.

Bibliography

[1] HFLAV, Y. Amhis *et al.*, *Averages of b-hadron, c-hadron, and τ-lepton properties as of summer 2016*, Eur. Phys. J. C **77** (2017) 895, arXiv:1612.07233.

[2] LHCb, R. Aaij *et al.*, *Observation of CP Violation in Charm Decays*, Phys. Rev. Lett. **122** (2019) 211803, arXiv:1903.08726.

[3] Particle Data Group, P. A. Zyla *et al.*, *Review of Particle Physics*, PTEP **2020** (2020) 083C01.

[4] R. H. Dalitz, *The $\tau - \theta$ puzzle*, AIP Conf. Proc. **300** (1994) 141.

[5] S. U. Chung *et al.*, *Partial wave analysis in K matrix formalism*, Annalen Phys. **4** (1995) 404.

[6] I. Bediaga *et al.*, *On a CP anisotropy measurement in the Dalitz plot*, Phys. Rev. D **80** (2009) 096006, arXiv:0905.4233.

[7] I. Bediaga *et al.*, *Second Generation of 'Miranda Procedure' for CP Violation in Dalitz Studies of B (\& D \& \tau) Decays*, Phys. Rev. D **86** (2012) 036005, arXiv:1205.3036.

[8] M. S. Sozzi, *Discrete symmetries and CP violation: From experiment to theory*, 2008.

[9] Fayyazuddin and Riazuddin, *Modern introduction to particle physics*, World Scientific, River Edge, N.J, 2012.

[10] T. D. Lee and C.-N. Yang, *Question of Parity Conservation in Weak Interactions*, Phys. Rev. **104** (1956) 254.

[11] C. S. Wu *et al.*, *Experimental Test of Parity Conservation in β Decay*, Phys. Rev. **105** (1957) 1413.

[12] R. L. Garwin, L. M. Lederman, and M. Weinrich, *Observations of the Failure of Conservation of Parity and Charge Conjugation in Meson Decays: The Magnetic Moment*

of the Free Muon, Phys. Rev. **105** (1957) 1415.

[13] L. Hadjiivanov, *Neutrino, parity violaton, V-A: a historical survey*, arXiv:1812.11629.

[14] G. Costa and G. Fogli, *Symmetries and group theory in particle physics. An introduction to space-time and internal symmetries*, vol. 823, 2012.

[15] M. Gell-Mann, *The Eightfold Way: A Theory of strong interaction symmetry*, .

[16] C.-N. Yang and R. L. Mills, *Isotopic spin conservation and a generalized gauge invariance*, .

[17] E. Fermi, *Tentativo di una teoria dell'emissione dei raggi beta*, Ric. Sci. **4** (1933) 491.

[18] F. L. Wilson, *Fermi's Theory of Beta Decay*, Am. J. Phys. **36** (1968) 1150.

[19] Gargamelle Neutrino, F. J. Hasert *et al.*, *Observation of Neutrino Like Interactions Without Muon Or Electron in the Gargamelle Neutrino Experiment*, Phys. Lett. B **46** (1973) 138.

[20] M. D. Schwartz, *Quantum Field Theory and the Standard Model*, Cambridge University Press, 2014.

[21] A. Pich, *Electroweak Symmetry Breaking and the Higgs Boson*, Acta Phys. Polon. B **47** (2016) 151, arXiv:1512.08749.

[22] Y. H. Ahn, H.-Y. Cheng, and S. Oh, *Wolfenstein Parametrization at Higher Order: Seeming Discrepancies and Their Resolution*, Phys. Lett. B **703** (2011) 571, arXiv:1106.0935.

[23] CKMfitter Group, J. Charles *et al.*, *CP violation and the CKM matrix: Assessing the impact of the asymmetric B factories*, Eur. Phys. J. C **41** (2005) 1, arXiv:hep-ph/0406184.

[24] J. H. Christenson, J. W. Cronin, V. L. Fitch, and R. Turlay, *Evidence for the 2π Decay of the K_2^0 Meson*, Phys. Rev. Lett. **13** (1964) 138.

[25] NA31, H. Burkhardt *et al.*, *First Evidence for Direct CP Violation*, Phys. Lett. B **206** (1988) 169.

[26] BaBar, B. Aubert *et al.*, *Evidence for $D^0 - \overline{D}^0$ Mixing*, Phys. Rev. Lett. **98** (2007) 211802, arXiv:hep-ex/0703020.

[27] BELLE, M. Staric *et al.*, *Evidence for D^0 - $\bar{D}^0$ Mixing*, Phys. Rev. Lett. **98** (2007) 211803, arXiv:hep-ex/0703036.

[28] CDF, T. Aaltonen *et al.*, *Evidence for $D^0 - \bar{D}^0$ mixing using the CDF II Detector*, Phys. Rev. Lett. **100** (2008) 121802, arXiv:0712.1567.

[29] LHCb, R. Aaij *et al.*, *Observation of $D^0 - \overline{D}^0$ oscillations*, Phys. Rev. Lett. **110** (2013) 101802, arXiv:1211.1230.

[30] BaBar, B. Aubert *et al.*, *Observation of CP violation in the B^0 meson system*, Phys. Rev. Lett. **87** (2001) 091801, arXiv:hep-ex/0107013.

[31] Belle, K. Abe *et al.*, *Observation of large CP violation in the neutral B meson system*, Phys. Rev. Lett. **87** (2001) 091802, arXiv:hep-ex/0107061.

[32] BaBar, B. Aubert *et al.*, *Observation of direct CP violation in $B^0 \to K^+\pi^-$ decays*, Phys. Rev. Lett. **93** (2004) 131801, arXiv:hep-ex/0407057.

[33] Belle, Y. Chao *et al.*, *Evidence for direct CP violation in B0 —> K+ pi- decays*, Phys. Rev. Lett. **93** (2004) 191802, arXiv:hep-ex/0408100.

[34] BaBar, P. del Amo Sanchez *et al.*, *Measurement of CP observables in $B^{+-}- > D_{CP}K^{+-}$ decays and constraints on the CKM angle γ*, Phys. Rev. D **82** (2010) 072004, arXiv:1007.0504.

[35] Belle, A. Poluektov *et al.*, *Evidence for direct CP violation in the decay B->D(*)K, D->KsPi+Pi- and measurement of the CKM phase phi3*, Phys. Rev. D **81** (2010) 112002, arXiv:1003.3360.

[36] LHCb, R. Aaij *et al.*, *Observation of CP violation in $B^\pm \to DK^\pm$ decays*, Phys. Lett. B **712** (2012) 203, arXiv:1203.3662, [Erratum: Phys.Lett.B 713, 351 (2012)].

[37] LHCb, R. Aaij *et al.*, *First observation of CP violation in the decays of B_s^0 mesons*, Phys. Rev. Lett. **110** (2013) 221601, arXiv:1304.6173.

[38] LHCb, R. Aaij *et al.*, *Measurements of CP violation in the three-body phase space of charmless $B^\pm$ decays*, Phys. Rev. D **90** (2014) 112004, arXiv:1408.5373.

[39] LHCb, R. Aaij *et al.*, *Amplitude analysis of $B^\pm \to \pi^\pm K^+ K^-$ decays*, Phys. Rev. Lett. **123** (2019) 231802, arXiv:1905.09244.

[40] C. Zemach, *Use of angular momentum tensors*, Phys. Rev. **140** (1965) B97.

[41] J. M. Blatt and V. F. Weisskopf, *Theoretical nuclear physics*, Springer, New York, 1952.

[42] F. Giacosa and G. Pagliara, *On the spectral functions of scalar mesons*, Phys. Rev. C **76** (2007) 065204, arXiv:0707.3594.

[43] J. R. Pelaez, *Light scalars as tetraquarks or two-meson states from large N(c) and unitarized chiral perturbation theory*, Mod. Phys. Lett. A **19** (2004) 2879, arXiv:hep-ph/0411107.

[44] LHCb, R. Aaij *et al.*, *Search for CP violation in $D^+ \to K^-K^+\pi^+$ decays*, Phys. Rev. D **84** (2011) 112008, arXiv:1110.3970.

[45] LHCb, J. Alves, A.Ãugusto *et al.*, *The LHCb Detector at the LHC*, JINST **3** (2008) S08005.

[46] LHCb, R. Aaij *et al.*, *LHCb Detector Performance*, Int. J. Mod. Phys. A **30** (2015) 1530022, arXiv:1412.6352.

[47] R. Aaij *et al.*, *Performance of the LHCb Vertex Locator*, JINST **9** (2014) P09007, arXiv:1405.7808.

[48] LHCb Outer Tracker Group, P. d'Argent *et al.*, *Improved performance of the LHCb Outer Tracker in LHC Run 2*, JINST **12** (2017) P11016, arXiv:1708.00819.

[49] LHCb RICH Group, M. Adinolfi *et al.*, *Performance of the LHCb RICH detector at the LHC*, Eur. Phys. J. C **73** (2013) 2431, arXiv:1211.6759.

[50] J. Alves, A.Ã. *et al.*, *Performance of the LHCb muon system*, JINST **8** (2013) P02022, arXiv:1211.1346.

[51] R. Aaij *et al.*, *The LHCb Trigger and its Performance in 2011*, JINST **8** (2013) P04022, arXiv:1211.3055.

[52] J. Back *et al.*, *LAURA^{++}: A Dalitz plot fitter*, Comput. Phys. Commun. **231** (2018) 198, arXiv:1711.09854.

[53] R. Brun and F. Rademakers, *ROOT - An Object Oriented Data Analysis Framework*, Nucl. Inst. Meth. in Phys. Res. A **389** (1997) 81, See also ROOT [software], Release v6.18/02, 23/08/2019.

[54] CLEO, P. Rubin *et al.*, *Search for CP Violation in the Dalitz-Plot Analysis of D+- —> K+ K- pi+-*, Phys. Rev. D **78** (2008) 072003, arXiv:0807.4545.

[55] G. Choudalakis and D. Casadei, *Plotting the Differences Between Data and Expectation*, Eur. Phys. J. Plus **127** (2012) 25, arXiv:1111.2062.